Plate Heat Exchangers Using Natural Graphite Sheets

by

Pouya Jamzad

B.Sc., Sharif University of Technology, 2015

Thesis Submitted in Partial Fulfillment of the
Requirements for the Degree of
Master of Applied Science

in the
School of Mechatronics System Engineering
Faculty of Applied Sciences

SIMON FRASER UNIVERSITY

Summer 2017

Approval

Name:	**Pouya Jamzad**
Degree:	**Master of Applied Science**
Title:	***Potentials of fabrication and utilization of natural flake graphite-based heat exchangers***

Examining Committee: Chair**: Mohammad Narimani**

Majid Bahrami
Senior Supervisor
Professor

Kevin Oldknow
Internal examiner
Senior lecturer

Gary Wang
Internal Examiner
Professor

Date Defended: July 31, 2017

Abstract

Graphite heat exchangers (G-HEX) are good alternatives to metallic heat exchangers due to their excellent thermal properties, low cost, light weight, and high resistivity to corrosion. In this study, the potential of fabrication of natural flake graphite-based plate heat exchanger is being investigated. A new layered G-HEX and a graphite plate heat exchanger are fabricated and their thermal and hydraulic performance are compared with an off-the-shelf chevron-type plate heat exchanger using a custom-made experimental setup. An optimization study is then conducted to further improve the graphite plate heat exchanger performance. To understand the potential of utilization of G-HEX in corrosive environments, a corrosion test is then performed on natural flake graphite sheets.

Keywords: Natural flake graphite; Fabrication method; Plate heat exchanger; Corrosion; Optimization

I would like to dedicate my thesis to my beloved family

Acknowledgements

I wish to thank my senior supervisor, Dr. Majid Bahrami for his great support, valuable guidance, and encouragements. It was an honor for me to work under his supervision at the Laboratory for Alternative Energy Conversion (LAEC).

I also thank my senior colleagues; Dr. Mehran Ahmadi and Dr. Wendell Huttema who helped me a lot during my study with their knowledge and valuable experience.

I like to also thank all the LAEC lab members for their great support and valuable memories during my research.

At the end I like to thank my family for their kind support and encouragements in all the moments of my life.

Table of Contents

List of Tables

List of Figures

Glossary

L_w	Plate width (m)
L_p	Plate length (m)
$\emptyset$	Enlargement factor
β	Chevron angel
$\dot{q}$	Heat transfer rate (W)
A	Heat transfer surface area (m2)
ΔT_M	Log mean temperature difference (K)
$\mathrm{T_{h,i}}$	Hot water inlet temperature (K)
$\mathrm{T_{h,o}}$	Hot water outlet temperature (K)
$\mathrm{T_{c,i}}$	Cold water inlet temperature (K)
$\mathrm{T_{c,o}}$	Cold fluid outlet temperature (K)
h_c	Convective heat transfer coefficient of cold water ($W.m^{-2}.K^{-1}$)
h_h	Convective heat transfer coefficient of hot water ($W.m^{-2}.K^{-1}$)
t_{plate}	Thickness of the plate (m2)
k_{plate}	Thermal conductivity of plate ($W.m^{-1}.K^{-1}$)
D_h	Hydraulic diameter (m)
k	Thermal conductivity of water ($W.m^{-1}.K^{-1}$)
ρ	Density of water ($kg.m^{-3}$)
v	Velocity of water ($m.s^{-1}$)
μ	Dynamic viscosity of water ($N.s.m^{-2}$)
Pr	Prandtl number
f	fanning friction factor
N	Number of channels
$\dot{m}$	Mass flow rate of water ($kg.s^{-1}$)
$A_{channel}$	Surface area of the channel (m^2)
A_{port}	Surface area of the port (m^2)
$\dot{V}_h$	Volumetric mass flow rate of water in hot side ($m^3.s^{-1}$)
$\dot{V}_c$	Volumetric mass flow rate of water in cold side ($m^3.s^{-1}$)
COP	Coefficient of performance

Executive Summary

Motivations

Heat exchangers are widely used in industrial applications such as power plants, geothermal facilities, chemical and food processing, automotive, power electronics, telecom, aerospace, heating, ventilating, air conditioning (HVAC) systems, and nuclear power generation. With the ever-growing need for energy, their significance has been increased in recent decades. The market size of heat exchanger is estimated to grow from USD 13.89 Billion in 2017 to USD 20.65 Billion by 2022 [1]. Design and material selection for heat exchangers are among the most important tasks in determining their performance, durability, and reliability. Conventionally heat exchangers are made from metallic alloys such as aluminum, steel, and copper due to their high thermal conductivity, manufacturability, and relatively low cost. However, these heat exchangers are heavy, prone to corrosion, and thermal shocks shortens their life.

Natural graphite is a corrosion-resistant material and has an exceptionally high thermal conductivity (300-600 $W.m^{-1}.K^{-1}$ in the in-plane direction vs aluminum 200 $W.m^{-1}.K^{-1}$), low density (2.1 $g.cm^{-3}$ vs. aluminum 2.7 $g.cm^{-3}$), and negligible coefficient of thermal expansion. These properties make graphite an excellent material for applications in energy conversion systems, electronics cooling, heat exchangers, HVAC systems, and automotive components. Artificial graphite has been used in heat exchanger industry. However, the high manufacturing cost of thermal products made from artificial graphite has been a significant obstacle preventing widespread adoption of them. Roll-embossing process enables cost-effective mass production of natural graphite thermal products with a significant lower manufacturing and material cost.

With the unique properties, graphite heat exchangers (G-HEX) made using rolled graphite sheets can be potentially used in corrosive environments such as power plants, geothermal facilities, and chemical processing. They can also be used in applications where there is a high temperature difference between hot and cold media such as liquid natural gas (LNG) and cryogenic vaporizers. Furthermore, considering cost-effectiveness and ease-of-manufacturing of graphite sheets in roll embossing, fabrication of G-HEX can be rapid and economical. This study is focused on investigation, design, fabrication, and utilization of G-HEX made from rolled graphite sheets.

Objectives

The research objectives are:

- To design and fabricate compact heat exchangers from rolled natural flake graphite sheets;
- To evaluate the performance of G-HEX and compare it with the typical off-the-shelf heat exchangers;
- To further improve the performance of a graphite plate heat exchanger by finding optimum value for design parameters; and
- To evaluate the corrosion resistivity of natural flake graphite sheets.

Methodology

In this thesis, a layered G-HEX and a graphite plate heat exchanger were designed, fabricated, and tested. A new custom-designed heat exchanger testbed was used to test the performance of the heat exchangers. The heat transfer rate, pressure drop, and U-value of the heat exchangers were compared to conventional heat exchangers in the testbed. An overview of the thesis and the research roadmap is shown in the figure below.

A new numerical model of the layered heat exchanger was developed in COMSOL MULTIPHYSICS 5.2a and validated with the experimental results. The results showed an 8.5% improvement in overall heat transfer coefficient of the designed GHEX when compared to the aluminum heat exchanger. This means that the layered graphite heat exchanger, with the same heat transfer surface area of the aluminum one, has 8.5% higher heat transfer rate.

To further improve the performance of the graphite plate heat exchangers, an optimization study was conducted on the design parameters of a chevron-type G-HEX. To establish the relationship between the design parameters, heat transfer, and pressure drop, a commercially available heat exchanger was tested in the heat exchanger testbed. The results were compared to available correlations of Nusselt number and friction factor inside the plate heat exchanger, and the most accurate ones were used in the optimization code. Utilizing genetic algorithm of MATLAB R2013b, the optimum value for each design parameter was found. Results showed an increase in surface goodness factor (a non-dimensional factor for heat transfer benefit over pressure drop cost) to that of the off-the-shelf plate heat exchanger.

The corrosion resistivity of rolled graphite sheets was evaluated experimentally through a one-week test in 98% concentration of sulfuric acid in the temperature of 25°C. The results proved that natural graphite is resistant to corrosion even in high concentration of sulfuric acid.

Contributions

The contributions of the present study are highlighted below:

- Fabrication, numerical simulation, and performance evaluation of a new layered G-HEX [30],
- Optimization study on the design parameters of a chevron-type plate heat exchanger,
- Studying the corrosion resistivity of rolled natural flake graphite sheets in sulfuric acid.

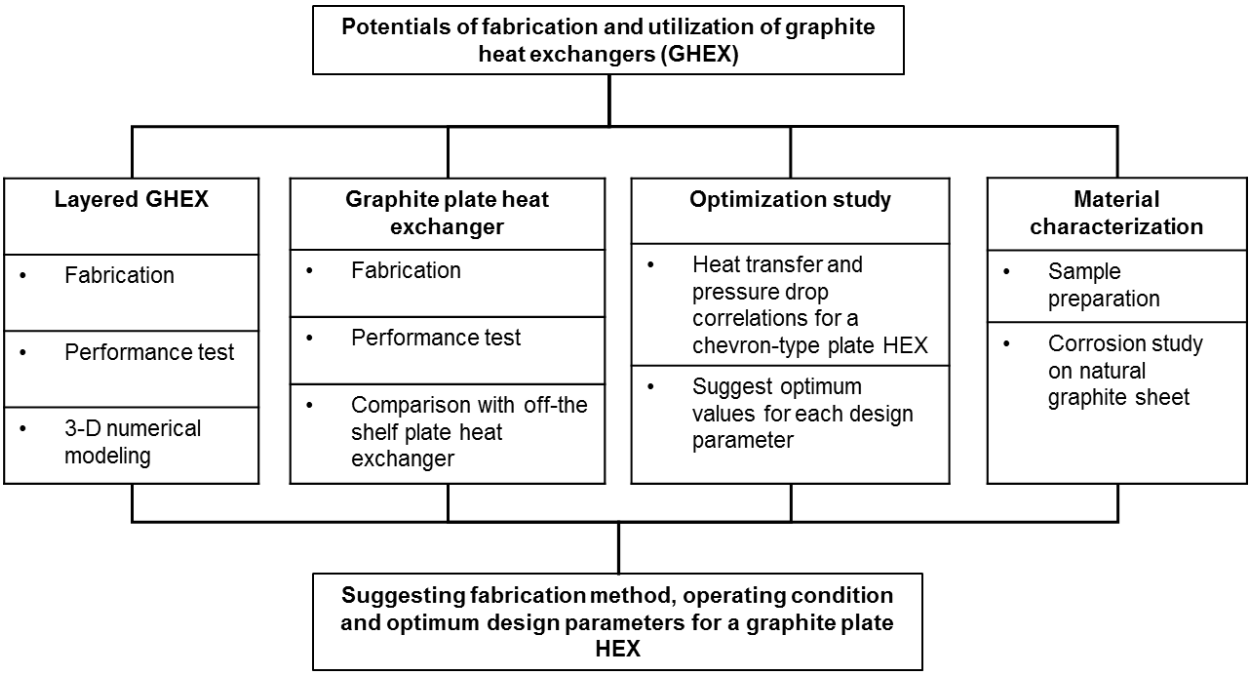

Present research road map

Chapter 1. Introduction

1.1 Research importance

Heat exchanger is a device that transfers the heat between a hot and a cold medium that can be in forms of gas, liquid, or two phase flow. Heat exchangers have been extensively used in applications such as oil and gas industry, food and chemical processing, power generation, refrigeration, and air conditioning systems. Due to fast industrialization, rise in energy needs, and developments in chemical, petrochemical and HVAC systems, the market need for heat exchangers has been constantly increased. The market value is estimated to grow from USD 13.89 Billion in 2017 to USD 20.65 Billion by 2022 [1].

In terms of performance of a heat exchanger, it is important to have the maximum heat transfer with the lowest pressure drop, size, and fabrication cost. Also in terms of maintenance costs, the durability and reliability of the heat exchangers is extremely important. They can be damaged by corrosion, erosion, thermal expansion, vibration, and thermal shocks [2, 3].

In any heat exchanger, other than design considerations, material selection plays a crucial role in determining its maintenance cost and life span. For example, heat exchangers made from a material with high coefficient of thermal expansion, are more likely to damage from thermal expansion. This damage type is common where there is a high temperature difference between the hot and cold fluid, such as cryogenic vaporizers. Also, the tendency of the material to react with corrosives directly determines its resistance to corrosion damage. Heat exchangers in urban air conditioning systems, process of flue gas, and chemical and petroleum processing can be subjected to this type of damage [4].

Conventional heat exchangers are made from metallic alloys, such as aluminum, copper, and steel. These alloys have good heat transfer properties, such as high thermal conductivity, and are easy to form and relatively cheap. However, aluminum, copper, and especially steel can all corrode in some extent when subjected to corrosive environments.

Rolled natural flake graphite sheets have interesting thermal properties such as a high in-plane thermal conductivity (300~600 $W.m^{-1}.K^{-1}$), low density (2.1 $g.cm^{-3}$), high resistivity to corrosion and negligible coefficient of thermal expansion. Compared to aluminum with thermal conductivity of 200 $W.m^{-1}.K^{-1}$ and density of 2.7 $g.cm^{-3}$, graphite is suitable for fabrication of thermal management devices such as heat exchangers and heat sinks. This research is focused on fabrication of heat exchangers from rolled natural flake graphite.

1.2 Rolled natural flake graphite

Graphite, the most stable form of carbon is found naturally in form of flakes. Other than the natural form, it can be made artificially. The process of making artificial form of graphite was discovered first in 1896 by Edward Goodrich Acheson [5]. The artificial synthetic resin impregnated graphite is now being used by SGL Carbon Company and Group Carbone Lorraine to produce G-HEX under the brands DIABON® and GRAPHILOR®, respectively. Figure 1 shows a summary of the manufacturing process of artificial graphite. In this process, low-iron petroleum coke and pitch binders are first mixed. The mixture is then formed by extrusion, molding, or pressing. After the formation, it is baked at 1200°C to create a non-deformable carbon body. Then at the graphitizing step, it is heated up to 3000°C by electricity to induce crystalline graphite structure [8].

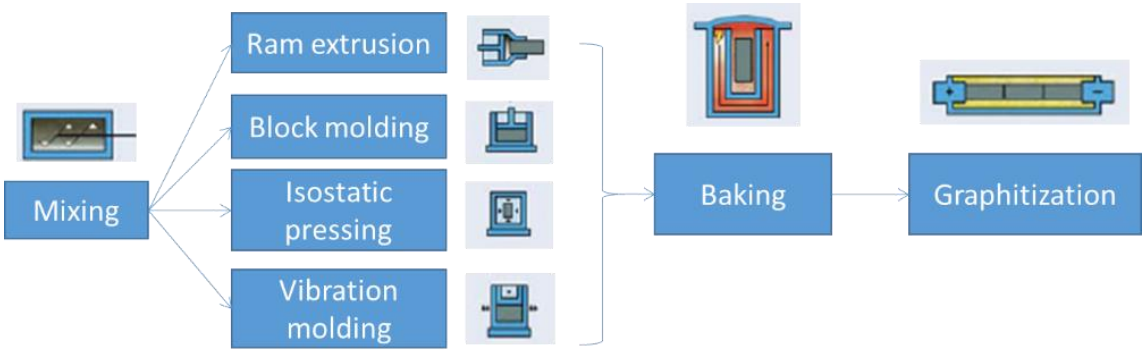

Figure 1. Manufacturing process of artificial graphite.

The fabrication cost of such heat exchangers is extremely high compared to metallic ones. For example, for cooling capacity of 5 kW with 10 m^2 of heat transfer surface area, a DIABON® plate

heat exchanger costs $40,000 CDN [6]. Also, with the current technology, the resin impregnation process with phenolic resin or PTFE (polyterafluoroethylene) can take up to six months [7].

Flake graphite is the most geologically common variation of natural graphite. T be found in form of sheets. Usually the uncompressed natural graphite sheets are soft and have a low density. In a rolling process, the graphite sheets can be compressed with a rolling machine to increase their mechanical properties and density. The rollers can also have detailed patterns to create patterned graphite sheets. This process is called roll-embossing technique. Compared to machining the blocks of artificial graphite, graphite sheets that are formed with this technique has significantly lower material and fabrication cost. Figure 2 shows a graphite sheet that is patterned under rolling machine.

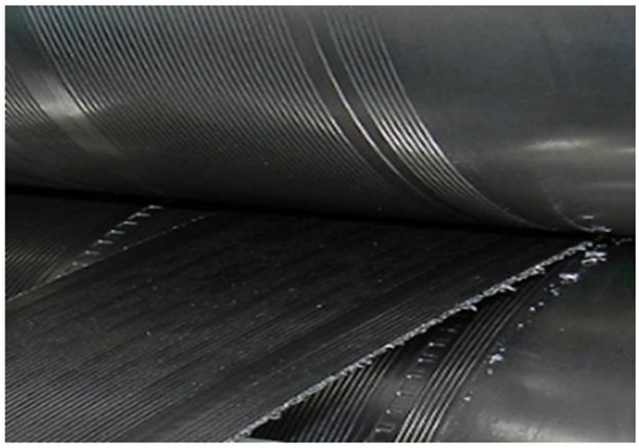

Figure 2. Roll-embossed natural graphite sheet

These sheets consist of a series of natural flakes that are mostly in horizontal direction. Figure 3 shows a Nano-SEM image of graphite flakes in a sheet taken by Nova NanoSEM 430. Carbon atoms in graphite flakes have strong covalent bonding in the in-plane direction and weak Van Der Waals bonding in the through-plane direction [9]. Thus the thermal conductivity of graphite flakes and accordingly graphite sheets is anisotropic. As mentioned, they have a high thermal conductivity in the in-plane direction (300~900 $W.m^{-1}.K^{-1}$) and a lower thermal conductivity (~5 $W.m^{-1}.K^{-1}$) in the through-plane direction.

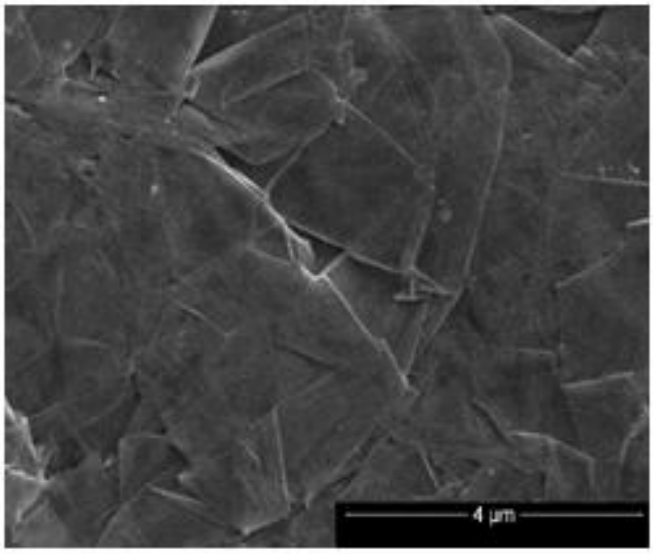

Figure 3. Nano SEM image of natural flake graphite sheet

1.3 Heat exchanger design criteria

As mentioned, heat exchanger is a device that transfers the heat between a hot and a cold medium. The high-temperature fluid loses its heat as it flows through the heat transfer area. Heat exchangers vary in size and design, based on their application. The most common types are plate-fin, plate, tube-tube, and shell-tube heat exchangers.

The heat transfer fluids can be in forms of gas, liquid, or two-phase flow, and the heat transfer can happen through evaporation, condensation, or a single-phase heat transfer between the fluids. As the mediums flow through the heat exchanger, they are subjected to pressure drop. Designers aim to maximize the heat transfer rate as well as achieving the minimum pressure drop. In general, the heat transfer rate of a heat exchanger is dependent on: thermal conductivity of the heat exchanger and heat transfer mediums, convective heat transfer coefficient of mediums, temperature difference between the hot and cold medium, and the surface area of the heat exchanger. For a specific application, for example, cooling hot oil with cold water, thermal conductivity of the fluids and the temperature difference between them are fixed parameters. A thermally effective heat exchanger, has a high thermal conductivity, increases the convective coefficient of the fluids, and provides a high surface area.

Other than thermal and hydraulic performance, manufacturability, cost, and size of the heat exchanger are other important design criteria. A summary of the design criteria is shown in Figure 4.

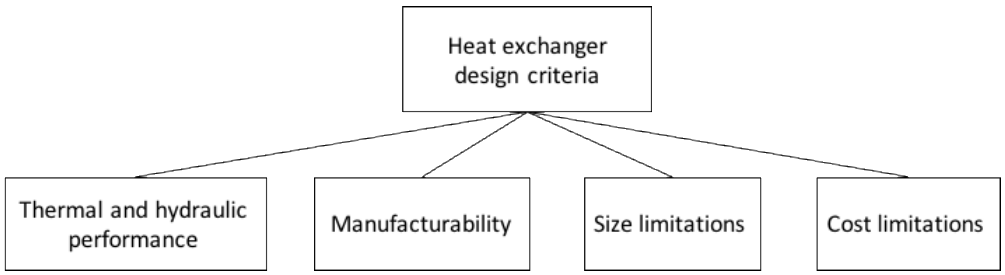

Figure 4. Heat exchanger design criteria.

There are no available literature on fabrication of G-HEX from rolled graphite sheets. As mentioned, graphite sheets have anisotropic thermal properties, including a high in-plane thermal conductivity. A novel fabrication method is to stack the layers of graphite sheets with specific cuts to form long channels for heat transfer fluids. Figure 5 shows the concept of layered G-HEX design.

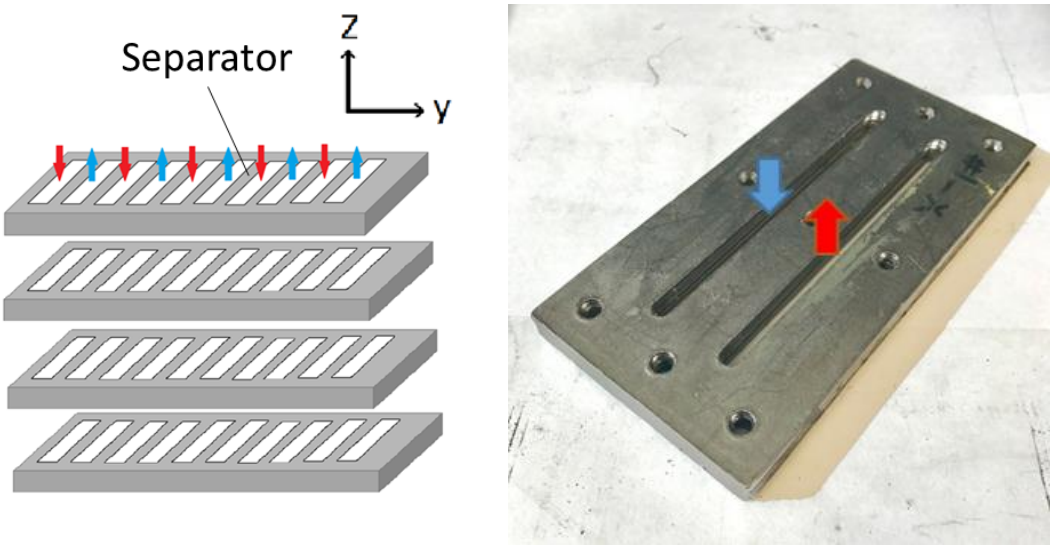

Figure 5. a) Concept of layered G-HEX design b) Example of a layered G-HEX

The blue and red arrows are used to indicate the hot and cold stream path, respectively. As it is shown, the heat transfer between the two mediums happens in the “y” direction through a graphite separator, where the thermal conductivity of the material is high. Although having a high in thermal conductivity, the main challenge in fabrication of this heat exchanger is the sealing between layers of graphite. All the layers of graphite needs to perfectly attached on top of each other, so that the hot/cold fluid do not mix up through the separator.

Epoxy can be used to seal the layers of graphite. In this case, if the separator thickness is low, it is challenging to seal many thin separators. So with the use of epoxy for sealing, the thickness of the separator between the hot and cold fluid cannot be very low to prevent the mixture of both streams. But in order for the heat exchanger to be compact, it should a high heat transfer surface area within its volume. Considering a thick separator between heat transfer fluids, a layered heat exchanger with high surface area and number of channels may become large in size and have a low compactness. Instead of epoxy, use of gasket for sealing the graphite layers would also lead to the bulkiness of the heat exchanger.

Another method for fabrication of G-HEX is to put sheets parallel to each other with gaskets in between them, so that the hot and cold streams flow in vertical channels. This is similar to conventional plate heat exchanger design. The gaskets in this case, in addition to sealing, create channels for the hot and cold fluid. The concept of this method is shown in Figure 6.

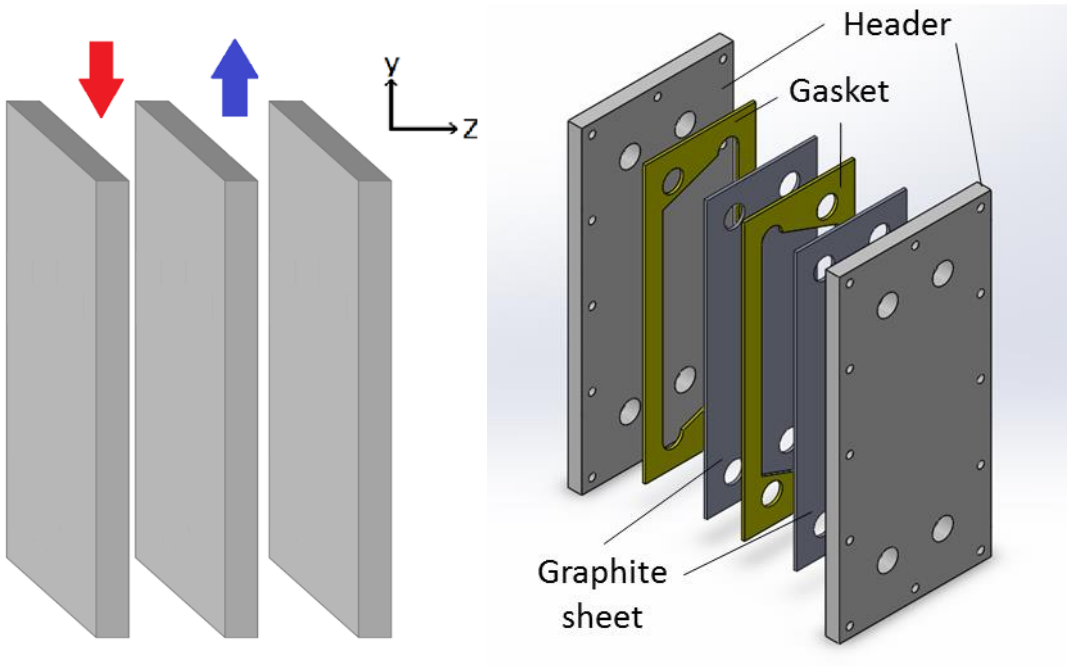

Figure 6. a) Concept of graphite plate heat exchanger design b) Example of graphite heat exchanger design

In this design, the heat transfer occurs in the through-plane ("z") direction, where the thermal conductivity is low; however, the channels can be narrow and long without having sealing issues. This can provide a high surface area for the heat transfer and increase the total heat transfer rate. To get the maximum heat transfer while having a minimum pressure drop, there are several design parameters that need to be considered and optimized for a plate heat exchanger design.

1.3.1 Literature review on plate heat exchanger design

Plate heat exchangers are categorized as compact heat exchangers providing a high heat transfer surface area per volume. In plate heat exchangers, the thin plate that transfers heat between the hot and cold fluid is usually patterned. More than 60 different surface patterns have been developed throughout the last century. Among these, chevron patterns are the most

commonly used by the manufacturers. They increase the heat transfer surface area, promote swirl flow, and disrupt the formation of boundary layers [10].

There are several geometrical design parameters for a chevron plate heat exchanger that can be seen in Figure 7. As shown, plate width, length, chevron angle, corrugation depth, and pitch are the design parameters of a plate heat exchanger. These parameters determine the heat transfer benefit between hot and cold fluid as well as the pressure drop cost.

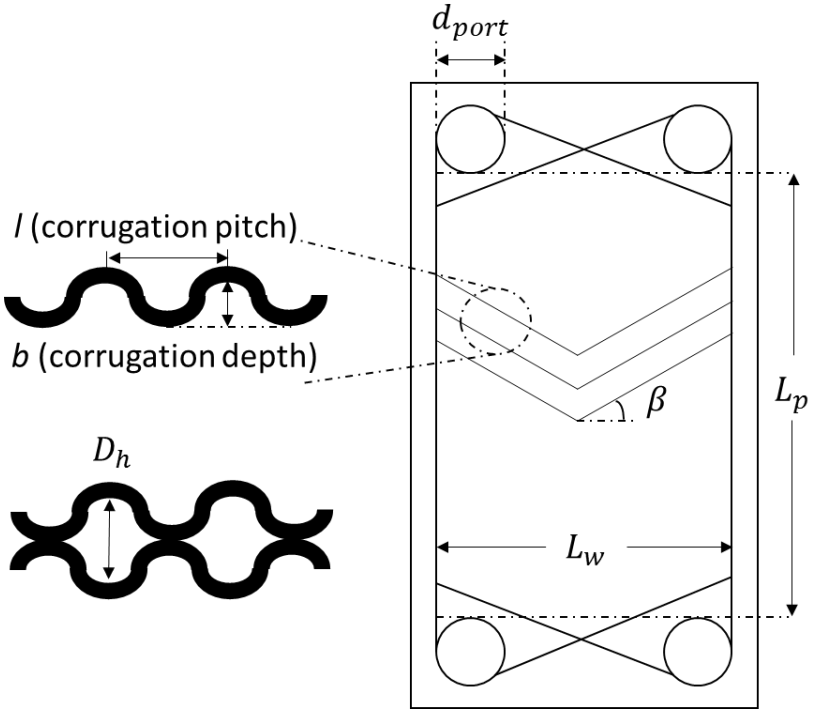

Figure 7. Design parameters of a chevron plate heat exchanger.

Researchers have analyzed the effect of each design parameter on heat transfer and pressure drop individually. A summary of their analysis is shown in Table 1.

Table 1. Summary of the literature review on the design parameters of a plate heat exchanger.

Ref.	Heat transfer fluid (Hot/Cold)	Reynlods number range	Design parameter	Remarks
A. Durmuş [11], (2009)	Water/Water	50 < Re < 1000	Plate surface profile	Compared heat transfer, pressure drop, friction factor, and exergy loss between asterisk, flat, and corrugated plate design
D. dovic [12], (2007)	Water-glycol/Water-glycol	0.1 < Re < 250	Corrugation aspect ratio, Chevron angle	Studied influence of aspect ratio and chevron angle on thermal-hydraulic performance of corrugated plates
J. Yin [13], (2012)	Air/Air	2000 < Re < 10000	Plate phase shift	Studied the effect of phase shift on flow and heat transfer in corrugated channels
G. A. Longo [14], (2008)	R-22/Water	350 < Re_w <1100	Surface roughness	Studied the effect of surface roughness on heat transfer coefficient and pressure drop during refrigerant vaporization

A. Durmus et al. investigated the effect of different surface profiles on heat transfer and pressure drop of plate heat exchangers experimentally, comparing flat, asterisk, and corrugated plates. They showed that the corrugated surface profile has a higher heat transfer rate due to induced turbulence as well as a higher pressure drop [11].

D. dovic et al. conducted experiment in two chevron angles of 28° and 61° and three aspect ratios (pressing depth / wave length) of 0.5, 0.4 and 0.27. They concluded that the higher chevron angle and aspect ratio lead to higher heat transfer and pressure drop [12].

J. Yin et al. investigated the influence of plate's shift angle (Figure 8) on heat transfer coefficient and frication factor of a plate heat exchanger. The shift angle defines the alignment of upper and lower corrugated plates relative to each other. They concluded that the highest heat transfer coefficient is obtained when ϕ=180° due to higher swirl recirculation of the fluid in channels [13].

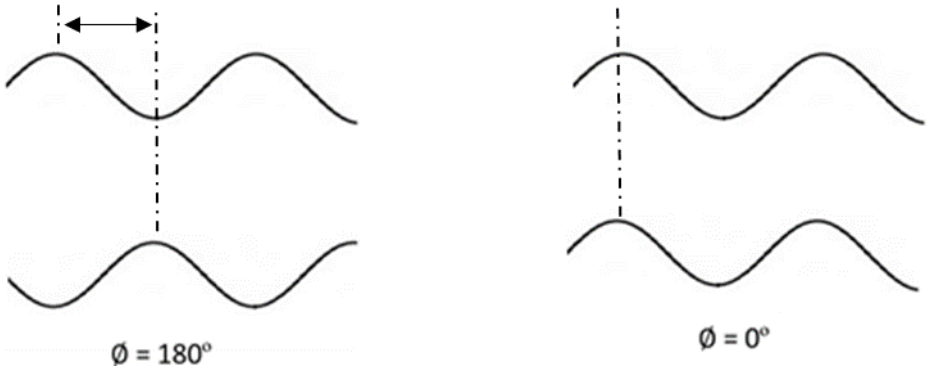

Figure 8. Plate shift angle.

G. A. Longo et al. investigated the effect of plate surface roughness and grooves on evaporation and condensation, experimentally. They showed that surface grooves can increase the heat transfer coefficient by 30-40% in vaporization and 60% in condensation. Whereas the increase in surface roughness showed a 30-40% increase in heat transfer coefficient only in vaporization [14].

To calculate the heat transfer and pressure drop prior to design, many researchers suggested experimental correlations to estimate Nusselt number and friction factor inside a chevron-type plate heat exchanger [21-25], where Nusselt number is the dimensionless form of convective heat transfer coefficient and the friction factor determines the energy loss due to friction. These correlations, however, differ in predicting the values of Nusselt number and friction factor. Some do not include all the geometrical parameters and are limited to certain ranges of Reynolds numbers. A summary of the Nusselt number and friction factor coefficients is shown in Table 2.

Table 2. Summary of the literature review on Nusselt number and friction factor coefficient for chevron-type plate heat exchanger

Ref.	Re number	Chevron angle	Correlation
Chisholm [15], 1992	100< Re < 10^4	30° < β < 80°	$Nu = 0.72Re^{0.59}Pr^{0.4}\emptyset^{0.41}(\beta/30)^{0.66}$ $f = 0.08Re^{-0.25}\emptyset^{1.25}(\beta/30)^{3.6}$
Martin [16], 1996	Re> 2000	10 ° < β < 80°	$Nu = 0.205Pr^{\frac{1}{3}}\left(\frac{\mu_m}{\mu_w}\right)^{\frac{1}{6}}(fRe^2\sin(2\beta))^{0.374}$ $\frac{1}{\sqrt{f}} = \frac{cos\beta}{\sqrt{0.045tan\beta + 0.09sin\beta + f_0/cos\beta}} + \frac{1-cos\beta}{\sqrt{3.8f_1}}$ $Re < 2000, f_0 = \frac{16}{Re}, f_1 = \left(\frac{149}{Re}\right) + 0.9625$ $Re > 2000, f_0 = (1.56lnRe - 3.0)^{-2}, f_1 = \frac{9.75}{Re^{0.289}}$
Maslov [17], 1972	Re < 2000 Re > 2000	$\beta = 60°$	$Nu = 0.63Re^{1/3}Pr^{1/3}$ $Nu = 0.78Re^{0.5}Pr^{1/3}$
Talik [18], 1995	10 < Re < 720 10 < Re < 80 1450 < Re < 11460	$\beta = 60°$	$Nu = 0.2Re^{0.75}Pr^{0.4}$ $f = 12.065Re^{-0.74}$ $Nu = 0.248Re^{0.7}Pr^{0.4}$ $f = 0.3323Re^{-0.042}$
Savostin, [19],1970	200 < Re/$\emptyset$ < 600	0 < β < 80°	$\boldsymbol{Nu = 1.26\,[0.62 + 0.38\cos(2.3\gamma)]\emptyset^{1-a1}Pr^{1/3}Re^{a1}}$ $\boldsymbol{f = 6.25(1 + 0.95\gamma^{1.72})\emptyset^{1.84}Re^{-0.84}}$ $\boldsymbol{a1 = 0.22[1 + \gamma^{1.5}]}$ $\boldsymbol{\gamma = 2\beta(radian)}$

Considering a range for the geometrical parameters of a plate heat exchanger, some studies focused on the optimization of each design parameter. V. Dvořák [20] used FLUENT CFD modeling with dynamic meshing to optimize the corrugation pitch in terms of pressure drop and efficiency. K. Guo [21] considered all the geometrical design parameters to minimize the capital cost of a plate heat exchanger using Martin's [16] Nusselt number and friction factor correlations. H. Khond et al. [22] focused on the minimization of the number of plates to meet the heat transfer and pressure drop requirements using a mathematical model suggested by Arsenyeva et al [23].

M. Kan et al. [24] used numerical modeling and experimental data to suggest the optimum chevron angle and mass flow rate to maximize the heat transfer rate. J.M. Pinto et al. [25] utilized a screening method to minimize the heat transfer area with constraints on the number of channels, pressure drop, mass flow rate, and effectiveness. A summary of the mentioned optimization studies is shown in Table 3.

Table 3. Summary of the literature review on optimization studies on the design parameters of chevron-type plate heat exchanger.

Ref.	**Optimization method/ tool**	**Optimization parameter**	**Design variables**
V. Dvořák [20], 2014	FLUENT CFD modeling	Heat transfer and pressure drop	Corrugation pitch
K.Guo [21], 2015	Nusselt number and friction factor correlations	Capital cost of plate heat exchanger	Plate length, width, chevron angle, plate spacing
H. Khond [22], 2016	Mathematical modeling	Heat transfer and pressure drop	Number of plates
M. Kan [24], 2016	Numerical modeling and experimental data	Heat transfer rate	Chevron angle and mass flow rate
J.M. Pinto [25], 2002	Screening method	Heat transfer area	Number of channels, mass flow rate

Based on the available literature, no study focused on maximization of surface goodness factor, which is a dimensionless parameter that shows the heat transfer benefit over pressure drop cost, considering all the design parameters. The surface goodness factor is mathematically defined in Eq. (11) [26].

The first step of this project suggests two fabrication methods for G-HEX made from the natural graphite sheets that are a layered G-HEX and a graphite plate heat exchanger. The thermal and hydraulic performance of the G-HEX are then compared to an off-the-shelf plate heat exchanger

using a custom-made single-phase water-water experimental setup. Then a numerical model of the G-HEX was built and validated with the experimental results.

As mentioned, one of the exceptional criteria of using G-HEX is in corrosive environments where most metallic heat exchangers fail to perform. To understand the potentials of graphite in highly corrosive environments, a set of corrosion tests were conducted on the natural flake rolled graphite. The next part of this research focused on corrosion test on graphite in highly corrosive environments. Graphite samples were placed in sulfuric acid with 98% concentration for duration of one week to monitor the potential changes in weight and surface features.

With the knowledge of manufacturability and applicability of rolled graphite sheets, the next step is to improve the thermal and hydraulic performance of the G-HEX. The optimization study of this work presented a set of values for geometrical design parameters that further improve the surface goodness factor and coefficient of performance of such heat exchangers. First a set of correlations for heat transfer and pressure drop calculation of a chevron-type heat exchanger were found from the literature. Then an experiment on an off-the-shelf plate heat exchanger was conducted to find the most accurate correlation. With the definition of the optimization parameters, upper and lower bounds and constraints, the correlations were then used in a MATLAB-based optimization code to find the optimum values of design parameters.

Chapter 2. Graphite heat exchanger prototyping

This chapter is focused on fabrication of two types of G-HEX; layered and plate heat exchanger. The material preparation process and fabrication steps are illustrated in details. To confirm that the heat exchanger can successfully operate without any leakage, leak test was performed after the fabrication.

2.1 Layered graphite heat exchanger

As mentioned in the introduction section, this heat exchanger is made from stacking graphite sheets. With this design, the hot and cold fluids transfer heat in the in-plane direction of graphite sheet, where the thermal conductivity is high. However, due to sealing and fabrication difficulties, this type of heat exchanger could not provide a high heat transfer surface area.

2.1.1 Fabrication steps

Flexible graphite sheet with area density of 140 $g \cdot cm^{-2}$ was first compressed down to 2mm with a rolling machine. After compression, the final density of graphite was increased to 1.4 $g \cdot cm^{-3}$. This also enhanced the mechanical properties of the sheets. Then sheets were mounted on a prepared cutting die and put under a hand press to cut into the desired shape. To further enhance the mechanical properties of graphite, the cut pieces went under the resin impregnation process for approximately 2 hours. The type of the resin was Hernon® Porosity Sealant (HPS) 991, a dimethacrylate blend.

The impregnated pieces were then stacked on top of each other using silicone adhesive sealant. To prevent leakage between hot and cold streams and between streams to environment, sealant was applied carefully around the flow stream path. Figure 9 shows the fabrication steps of layered G-HEX. A total of 30 pieces were stacked to form the final graphite block.

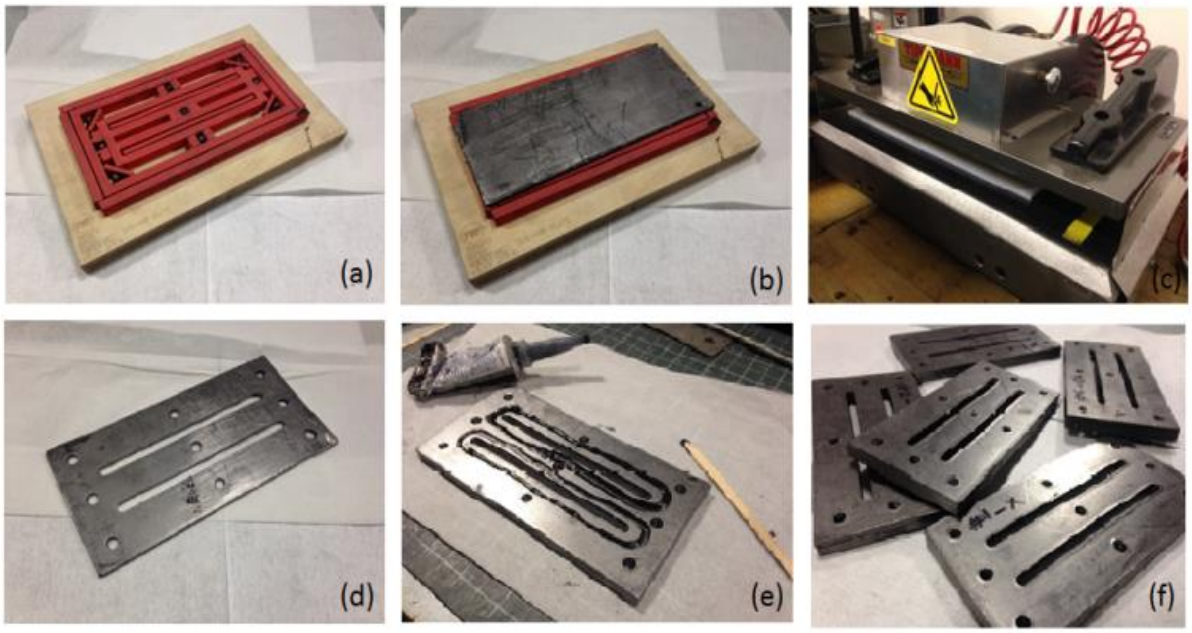

Figure 9. Fabrication steps of layered G-HEX: a) Preparation of cutting die, b) Mounting the layered graphite on cutting die, c) Cutting the layered graphite with hand press, d) Output of the press after resin impregnation, e) Applying adhesive sealant, and f) Stack of graphite layers.

Two identical headers were designed and fabricated via 3-D printing. The headers were attached to the ends of the graphite block to collect the flow from heating/cooling source and distribute it within the graphite block. To seal the contact between graphite block and headers, thin rubber sheets were cut and attached to the interface. Header and graphite block were held together using 9 bolts. Figure 10-a shows the final configuration of the heat exchanger and Figure 10-b shows its geometrical parameters. The value of each parameter is shown in Table 4.

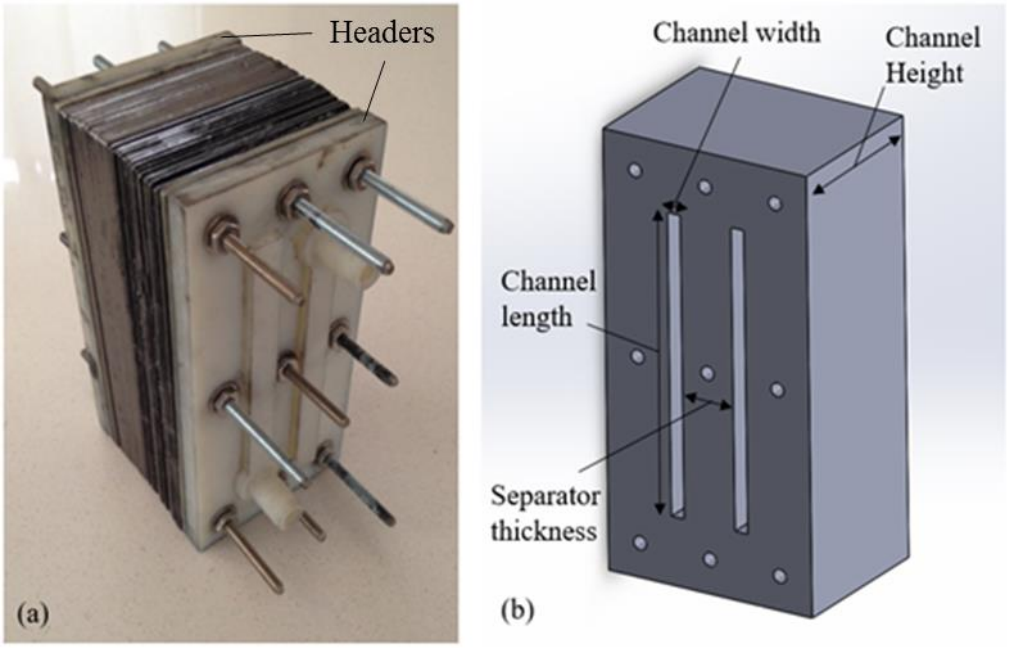

Figure 10. a) Final configuration of the assembled G-HEX, b) Geometrical parameters of the G-HEX.

Table 4. Geometrical parameters of the layered G-HEX

Geometrical parameter	Value (mm)
Channel length	110
Channel width	5
Channel height	60
Separator thickness	20

2.1.2 Leak test

To insure that the heat exchanger is properly sealed, a leak test experiment was conducted with air. In the designed setup, an air compressor was connected to the inlet of the hot/cold loop of the heat exchanger and its pressure was measured by a pressure gauge. The outlet was also blocked by another pressure gauge. Then the heat exchanger was submerged

into a water bath for leak detection. By increasing the compressor power, air pressure raised inside the heat exchanger. Since the outlet was blocked, any leak in the heat exchanger creates bubbles inside the water bath. Figure 11 shows a schematic of the leak test experimental setup.

The test showed that the G-HEX could operate up to 10 psi without any leak. Tightening the G-HEX bolts (between header and graphite block) can increase the operating pressure; however, it may cause the failure of 3-D printed headers. The bolts were tightened gradually and one by one until no leak was observed. Potentially, the use of a metallic header such as aluminum could increase the operating pressure of the G-HEX.

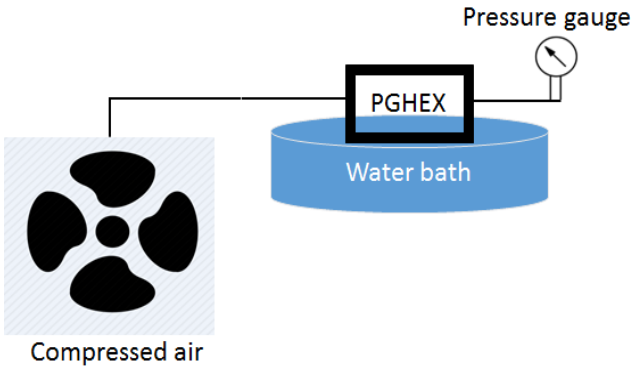

Figure 11. Schematic of the leak test experimental setup.

2.2 Graphite plate heat exchanger

As mentioned in the introduction, a plate heat exchanger consists of a series of plates and gaskets. The gaskets between the plates create a path for hot and cold fluid, and prevent the mixture of the fluids and leakage to the environment. The graphite plate heat exchanger design uses vertical graphite sheets to transfer heat between hot and cold fluid. This design provides a higher surface area compared to the layered G-HEX, is much easier to fabricate, and has no adhesives.

2.2.1 Fabrication steps

Similar to the layered G-HEX, first the 140 g·cm^{-2} graphite sheets were compressed down to 2mm to increase the density and mechanical strength. Then using cutting dies, graphite and rubber sheets were put under the hand press to form the plate and gaskets. Figure 12 shows the design cutting dies for plate and gasket. 10 plates and gaskets were cut for a 10-channel plate heat exchanger. Similar to the layered G-HEX in previous section, the plates then went through the same duration of resin impregnation process.

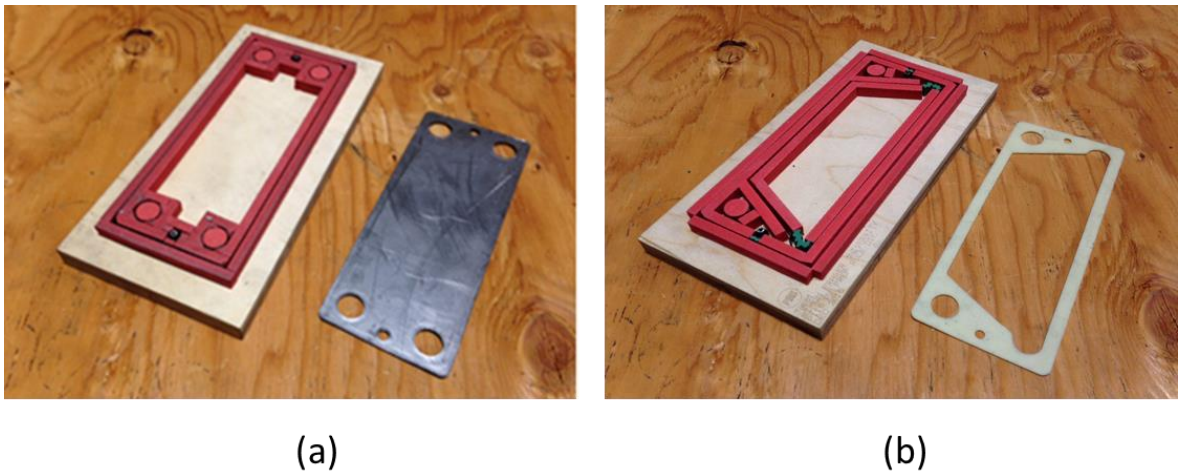

Figure 12. Cutting dies of graphite plate heat exchanger for: a) plate, and b) gasket.

Two aluminum headers were also designed and machined for both ends. With the use of aluminum headers instead of 3-D printed ones, the bolts were tightened more to provide a good sealing between the gasket and plates. Figure 13 shows the assembly steps in details.

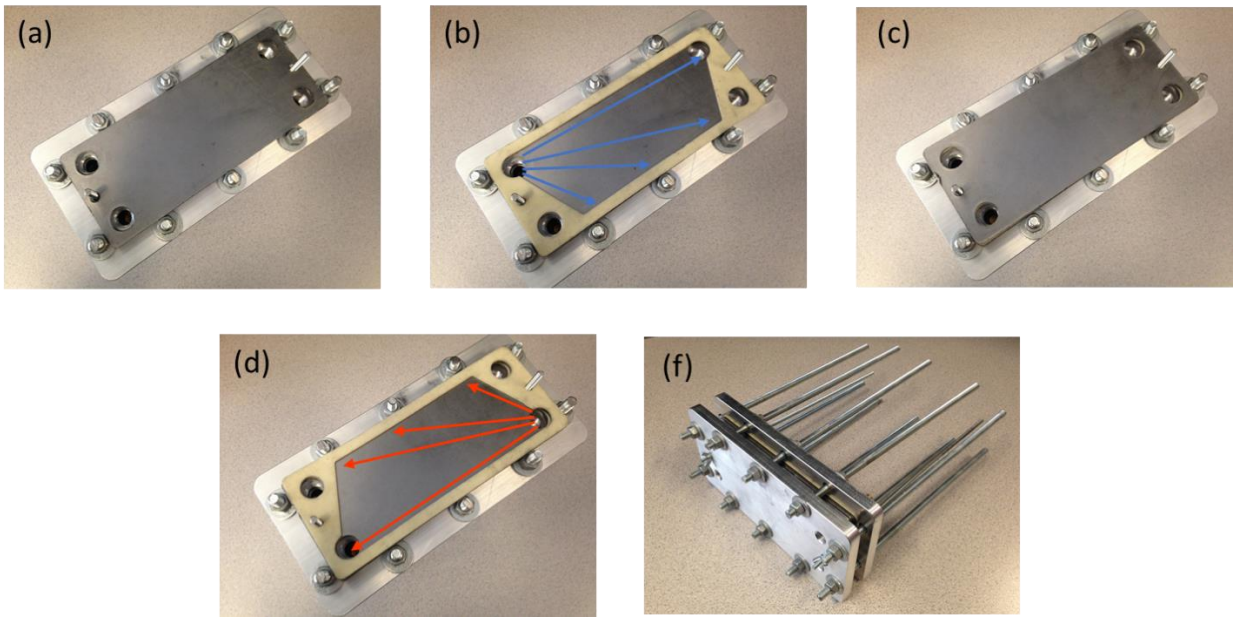

Figure 13. Assembly steps of a graphite plate heat exchanger: a) Mount the graphite sheet on the aluminum header, b) Put the first gasket (create a channel for cold fluid), c) Put another graphite sheet, d) Put the second gasket in the opposite direction (create a channel for hot fluid), f) Repeat the steps 10 times, put the second aluminum header

The geometrical parameters of this heat exchanger is shown in Table 5.

Table 5. Geometrical parameters of the graphite plate heat exchanger.

Geometrical parameter	Value (mm)
Plate width	80
Plate length	200
Gasket thickness	1.5
Number of channels	10

2.2.2 Leak test

The same experimental setup in section 2.1.2 was used for the leak test with the compressed air. After highly tightening the heat exchanger bolts, it was seen that the graphite plate heat exchanger could operate up to 50 psi without leaking, which was 5 times higher than the layered G-HEX.

Chapter 3. Heat exchanger performance evaluation

In this chapter, an experimental setup was designed and fabricated to evaluate the thermal and hydraulic performances of three heat exchangers: an off-the-shelf chevron-type plate heat exchanger; a layered G-HEX; and a graphite plate heat exchanger. After individual tests on each heat exchanger, their performances were compared.

3.1 Thermal and hydraulic performance

One of the most common methods for measuring the thermal performance of a heat exchanger is Logarithmic Mean Temperature difference (LMTD) method [26]. LMTD method is used to measure the overall heat transfer coefficient (U-value), based on the measurement of flow rates and inlet/outlet temperatures, as shown in Eq. (1). The equation can be derived with the assumptions of steady-state flow condition, constant specific heat of hot/cold streams with no phase change, constant flow raters, and a constant U-value [32, 33].

$$\dot{q} = UA\Delta T_m \tag{1}$$

Where:

$\dot{q}$= heat transfer rate (W)

U = U-value ($W.m^{-2}.K^{-1}$)

A = heat transfer area (m^2)

ΔT_m= logarithmic temperature difference between the fluids (K)

The ΔT_m represents the logarithmic average of the temperature difference of hot and cold fluids as shown in Eq. (2).

$$\Delta T_m = \frac{\Delta T_2 - \Delta T_1}{\log \Delta T_2 / \Delta T_1} \quad (2)$$

In the case of a counter flow heat exchanger:

$$\Delta T_1 = T_{h,i} - T_{c,o} \quad (3)$$

$$\Delta T_2 = T_{h,o} - T_{c,i}$$

Where:

$T_{h,i}$ = Hot fluid inlet temperature (K)

$T_{h,o}$ = Hot fluid outlet temperature (K)

$T_{c,i}$ = Cold fluid inlet temperature (K)

$T_{c,o}$ = Cold fluid outlet temperature (K)

The heat transfer rate can also be calculated with Eq. (4).

$$\dot{q} = \dot{m} c_p (T_{h,i} - T_{h,o}) \quad (4)$$

The U-value is defined as heat transfer per unit surface area and unit temperature difference. A higher U-value in a one heat exchanger compared to another shows that with the same heat transfer surface area and inlet fluids temperature difference, this heat exchanger is able to transfer more heat from hot fluid to the cold fluid. The U-value in a plate heat exchanger is related to convective heat transfer coefficient of the fluids as well as the conduction resistance of the plate as shown in Eq. (5). Then the Nusselt number in the plate heat exchanger can be driven from Eq. (5-7) [4].

$$\frac{1}{U} = \frac{1}{h_c} + \frac{1}{h_h} + \frac{t_{plate}}{k_{plate}} \quad (5)$$

Where:

h_c = Convective heat transfer coefficient of the cold fluid ($W.m^{-2}.K^{-1}$)

h_h = Convective heat transfer coefficient of the hot fluid ($W.m^{-2}.K^{-1}$)

t_{plate} = Thickness of the plate (m)

k_{plate} = Thermal conductivity of the plate ($W.m^{-1}.K^{-1}$)

$$Nu = \frac{hD_h}{k} \quad (6)$$

Where:

D_h= Hydraulic diameter (m)

k = Fluid thermal conductivity ($W.m^{-1}.K^{-1}$)

The hydraulic diameter of the plate heat exchanger can be approximated using Eq. (7) [4]. The hydraulic diameter can be seen in the Figure 7.

$$D_h = \frac{4A}{P} = \frac{4(b \times L_w)}{2(b + L_w)} \approx 2b \quad (7)$$

Where:

b= Corrugation pitch (channel spacing) (m)

L_w = Plate width (m)

The Reynolds number can be calculated using Eq. (8) [4].

$$Re = \frac{\rho v D_h}{\mu} \tag{8}$$

Where:

ρ= Density of water (kg.m^{-3})

v= Velocity of water (m.s^{-1})

μ= Dynamic viscosity of water (N.s.m^{-2})

The pressure drop of the plate heat exchanger can be calculated from Eq. (9). The first term on the left accounts for pressure drop inside the plate heat exchanger and the second term considers the pressure drop from the ports of the heat exchanger [24].

$$\Delta P = \frac{4 f L_p}{2\rho}\left(\frac{\dot{m}}{N.A_{channel}}\right)^2 + \frac{1.4}{2\rho}\left(\frac{\dot{m}}{A_{port}}\right)^2 \tag{9}$$

Where:

f= fanning friction factor

N= Number of channels

$\dot{m}$ = Mass flow rate of water (kg.s^{-1})

$A_{channel}$ = Surface area of the channel (m^2)

A_{port} = Surface area of the port (m^2)

3.2 Experimental setup

A custom-made experimental setup was designed to measure the U-value and pressure drop of heat exchangers. As shown in Figure 14, a heating and a cooling unit supplied the hot/cold water as the heat transfer fluids. These units kept a constant temperature for hot/cold inlets and pumped them inside the loops. For both loops, a control valve was provided to control the flow rate. A Coriolis flow meter was used for the flow rate measurement. For the temperature measurement, four thermocouples were put before/after the heat exchanger to measure the inlet/outlet temperatures. Also for the pressure drop measurement, two pressure transducers were used before and after each loop. The list of all the sensors with their accuracy is given in Table 6.

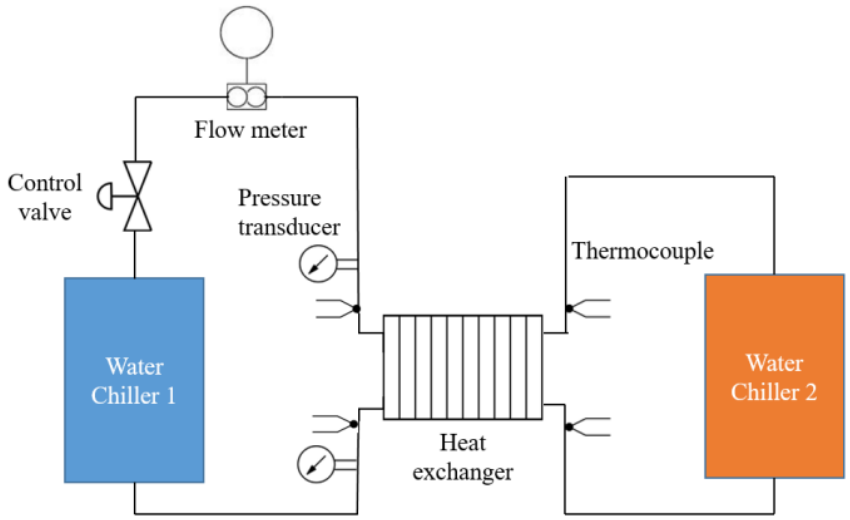

Figure 14. Schematic of the experimental setup.

Table 6. Experimental setup sensor information.

Sensor	Make	Accuracy	Measurement range
Thermocouple	Omega T type	±0.5°C	0 to 220°C
Pressure transducer	Omega PX305	0.25%	0 to 200 kPa
Flow meter	FLOMEC OM015S001	0.5%	1 to 40 lit.min^{-1}

For a more accurate measurement of temperatures, thermocouple connections were insulated. Surface of the heat exchangers were also carefully insulated to minimize the heat exchange to ambient. Ideally in the experiments all the heat transfer between hot and cold fluid happened should happen inside the heat exchanger. The experimental setup configuration and insulated parts are shown in Figure 15.

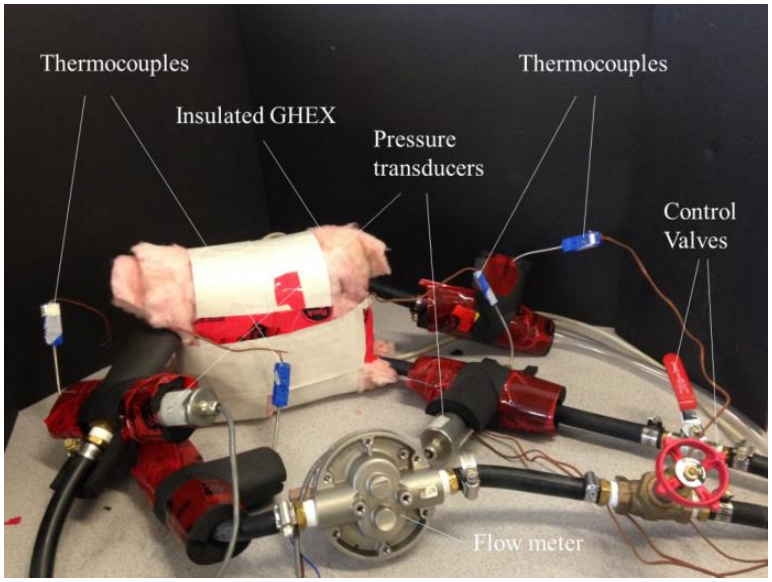

Figure 15. Experimental setup configuration.

3.3 Uncertainty analysis

In the measurement of the flow rate, Reynolds number, Nusselt number, pressure drop, and U-value using sensors are uncertainties that need to be considered. The uncertainties are calculated with following equations and the results are reported in Table 7 [26].

$$\frac{\delta U}{U} = \left(\left(\frac{\delta Q}{Q}\right)^2 + \left(\frac{\delta A}{A}\right)^2 + \left(\frac{\delta \Delta T_m}{\Delta T_m}\right)^2\right)^{\frac{1}{2}}$$

$$\frac{\delta Q}{Q} = ((\frac{\delta \dot{m}}{\dot{m}})^2 + (\frac{\delta \Delta T}{\Delta T})^2)^{1/2}$$

$$\frac{\delta \Delta T_m}{\Delta T_m} = ((\frac{\delta(\Delta T_1 - \Delta T_2)}{\Delta T_1 - \Delta T_2})^2 + (\frac{\delta \ln\left(\frac{\Delta T_1}{\Delta T_2}\right)}{\ln\left(\frac{\Delta T_1}{\Delta T_2}\right)})^2)^{1/2}$$

$$\delta \ln\left(\frac{\Delta T_1}{\Delta T_2}\right) = \frac{\delta\left(\frac{\Delta T_1}{\Delta T_2}\right)}{\left(\frac{\Delta T_1}{\Delta T_2}\right)}$$

$$\frac{\delta Re}{Re} = ((\frac{\delta v}{v})^2 + (\frac{\delta D_h}{D_h})^2)^{1/2}$$

$$\frac{\delta Nu}{Nu} = ((\frac{\delta h}{h})^2 + (\frac{\delta D_h}{D_h})^2)^{1/2}$$

$$\frac{\Delta f}{f} = ((\frac{\delta \Delta P}{\Delta P})^2 + (\frac{\delta L_P}{L_p})^2 + 4(\frac{\delta \dot{m}}{\dot{m}})^2 + 2(\frac{\delta A_{channel}}{A_{channel}})^2 + 2(\frac{\delta A_{port}}{A_{port}})^2)^{1/2}$$

Table 7. Uncertainty analysis results.

Measured parameter	Uncertainty (%)
U-value	7.4
Pressure drop	0.5
Flow rate	0.5
Nusselt number	8.8
Reynolds number	0.6
Fanning friction factor	1

The flow rate and pressure drop are directly calculated from the sensor measurements and therefore they have the lowest uncertainty. The Fanning frication factor and Reynolds number are calculated based on pressure transducer and flow meter measurements respectively. According

to Table 6, these sensors have a high accuracy compared to thermocouples. The Nusselt number and U-value, are calculated from the measurements of 4 thermocouples each with a 0.5°C uncertainty. Therefore, these parameters have a higher uncertainty. Since a 0.5°C uncertainty is common among thermocouples, the corresponding higher uncertainty of Nusselt number and U-value is acceptable and inevitable.

3.4 Layered graphite heat exchanger

In this section, the thermal and hydraulic performance of the layered G-HEX was measured via the experimental setup. The results were then compared and validated with a COMSOL-based numerical model. According to the numerical model, there was an increase in the graphite heat exchanger U-value compared to the identical aluminum version.

3.4.1 Experimental results

Water was used as the heat transfer fluid at a constant inlet temperature. The inlet temperature of the hot loop was set to 45ºC and the flow was set to a constant value of 1 lit·min^{-1}. On the cold loop, the temperature was set to 4.5ºC and the flow rate changed from 1 to 4.5 lit·min^{-1}. Summary of the inputs of the experiment is shown in Table 8.

Table 8. Inputs of the experimental study on the layered G-HEX.

Experiment inputs	Properties
Working fluid of hot and cold loop	Water
Hot fluid inlet temperature	45ºC
Cold fluid inlet temperature	4.5ºC
Hot fluid inlet flow rate	1 lit.min^{-1}
Cold fluid inlet flow rate	1~4.5 lit.min^{-1}

With the variation of the cold loop flow rate, inlet and outlet temperatures and pressures were measured. For each flow rate, the U-value was calculated using Eq. (1-3). Pressure drop

was reported by subtracting inlet and outlet pressures. The results of the U-value and pressure drop are shown in Figures 16 and 17, respectively.

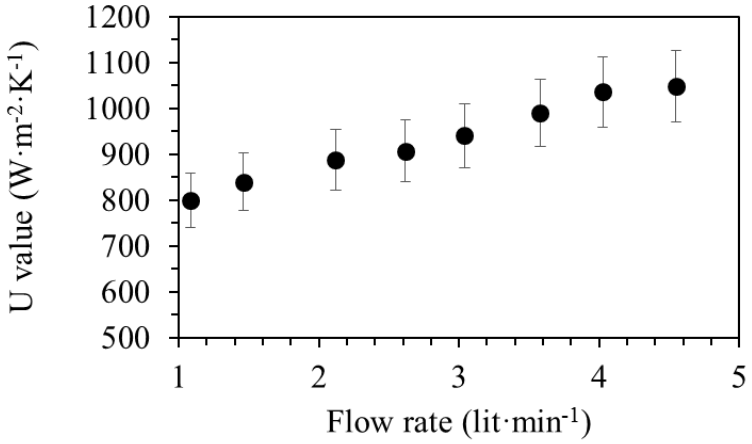

Figure 16. U-value variation with flow rate for layered G-HEX.

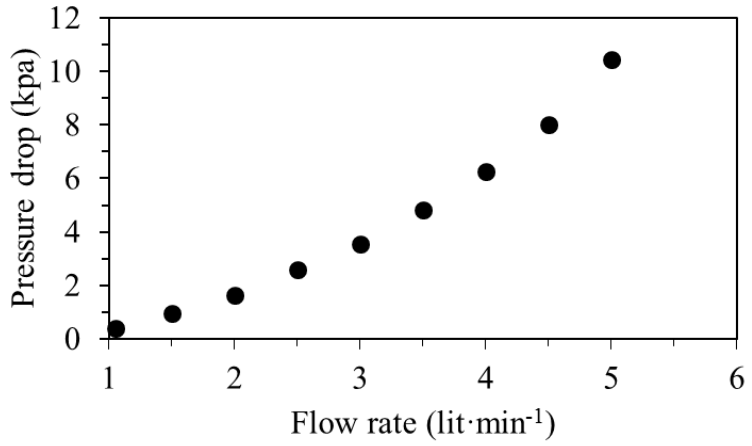

Figure 17. Pressure drop variation with flow rate for layered G-HEX.

The plot shows a constant increase in U-value with respect to flow rate. The U-value is a function of convective heat transfer coefficient of fluids and conduction resistance of graphite. The value of the convective heat transfer coefficient is proportional to the Reynolds number of flow [10]. Therefore, higher flow rates lead to a high Reynolds number, convective heat transfer coefficient, and U-value. The Reynolds number of the internal flow inside the channels was less than 2300 which shows that the flow was in laminar region [27].

Pressure drop also shows an increasing trend over flow rate. Also according to Eq. (8), in internal laminar flow, pressure drop is expected to increase with the power of 2 of the fluid velocity. The error bars for the pressure drop data were not visible due to the low uncertainty.

3.4.2 Numerical results

A 3-D numerical model was developed in COMSOL MULTIPHYSICS 5.2a with the same geometrical parameters of fabricated G-HEX. An insulation boundary condition was applied to the outer surface of the heat exchanger. For the inlet and outlet of the heat transfer fluid, boundaries were set to velocity inlet and pressure outlet, respectively. After a mesh independency analysis, a total number of 105241 tetrahedral meshes were used for the calculation of U-value. As shown in Figure 18, an increase in the number of elements after 10000 did not have an effect on the U-value. Also, the obtained results were in range of uncertainty of the experimental data that are shown in Figure 19.

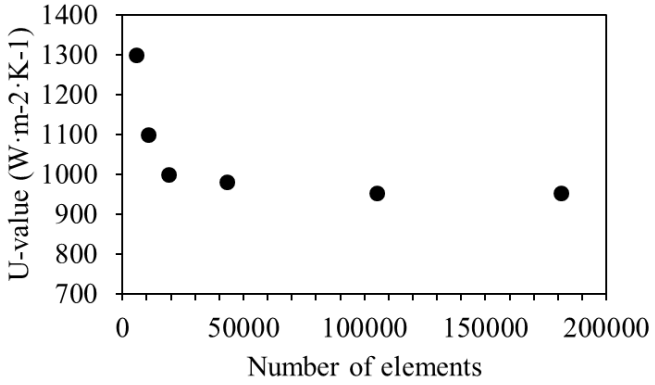

Figure 18. Mesh independency analysis

To compare the numerical results with the experimental study, the inputs of the model, such as hot and cold fluid inlet temperatures and flow rates were set equal to those from the experimental study, shown in Table 8. Other input parameters, including water and graphite physical and thermo-physical properties are indicated in Table 9 [27].

Table 9. Input parameters of the layered G-HEX numerical model.

Input parameters	Value
Density of water	998.2 $kg \cdot m^{-3}$
Specific heat of water	4182 $j \cdot kg^{-1} \cdot K^{-1}$
Thermal conductivity of water	0.6 $W \cdot m^{-1} \cdot K^{-1}$
Viscosity of water	0.001003 $N \cdot s \cdot m^{-2}$
Density of graphite	1400 $kg \cdot m^{-3}$
Specific heat of graphite	720 $j \cdot kg^{-1} \cdot K^{-1}$
In-plane thermal conductivity of graphite	300 $W \cdot m^{-1} \cdot K^{-1}$
Through-plane thermal conductivity of graphite	5 $W \cdot m^{-1} \cdot K^{-1}$

Assuming steady-state conditions and laminar flow, the output temperatures were obtained after each run. Similar to the experiment, the U-value was calculated in different mass flow rates as shown in Figure 19. The temperature and velocity profiles of the numerical model are also shown in Figure 20 and 21 respectively.

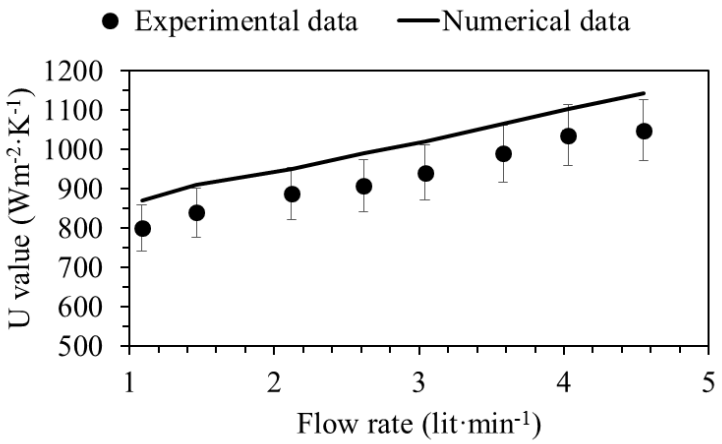

Figure 19. U-value variation with flow rate.

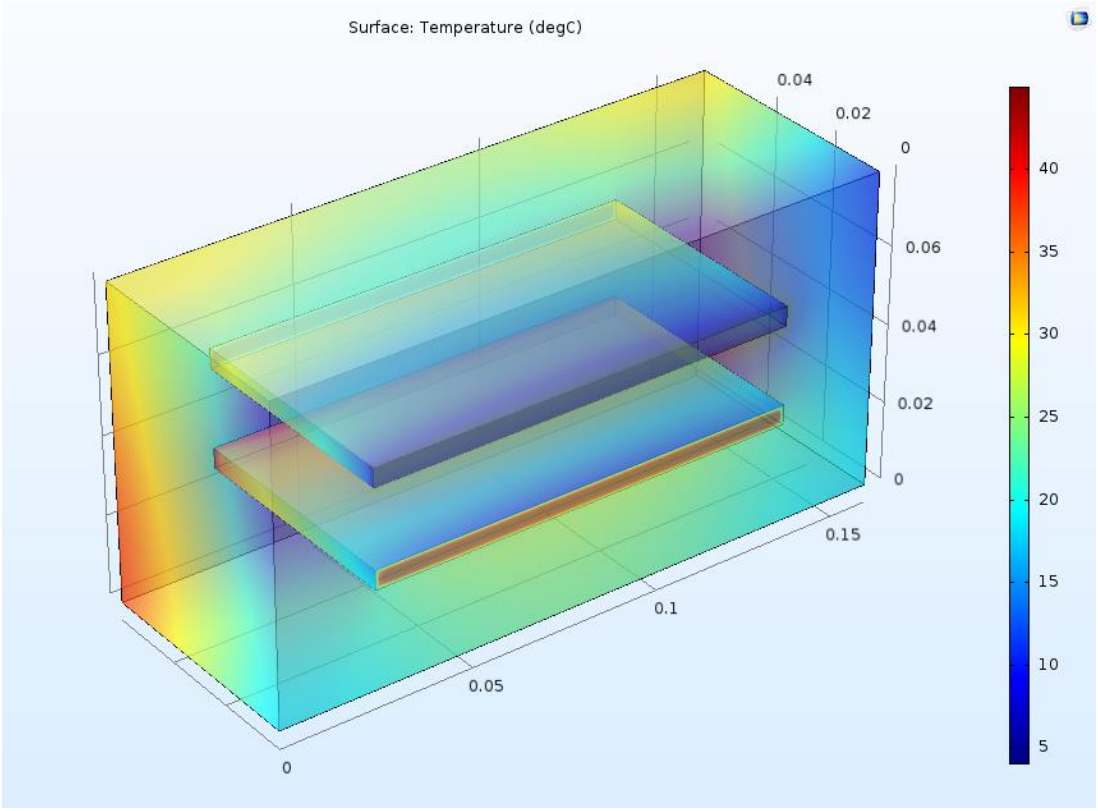

Figure 20. Temperature profile of the numerical model

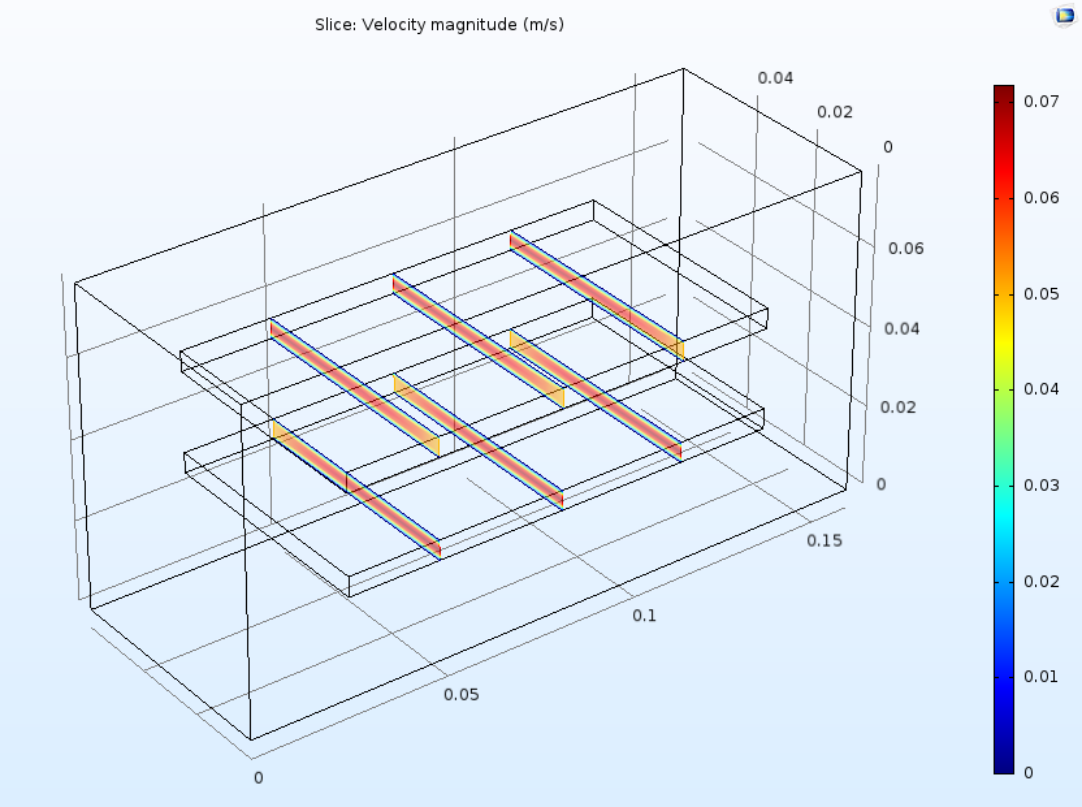

Figure 21. Velocity profile of the numerical model

The numerical results on variation of the U-value with respect to flow rate showed the same trend as the experimental study. The consistent difference between the numerical results and experimental data can be due to the imperfect insulation of the heat exchanger and connections in the experimental setup. However, the numerical model considers a perfect insulation boundary condition resulting in a higher U-value.

After validation of the model, a sensitivity analysis was performed to investigate the effect of input parameters on the U-value. The input parameters were changed from -30% to 30% of their original value and the corresponding U-value evaluated in the plot of Figure 19. This variation for the input parameters is common among different working fluids and heat exchanger materials.

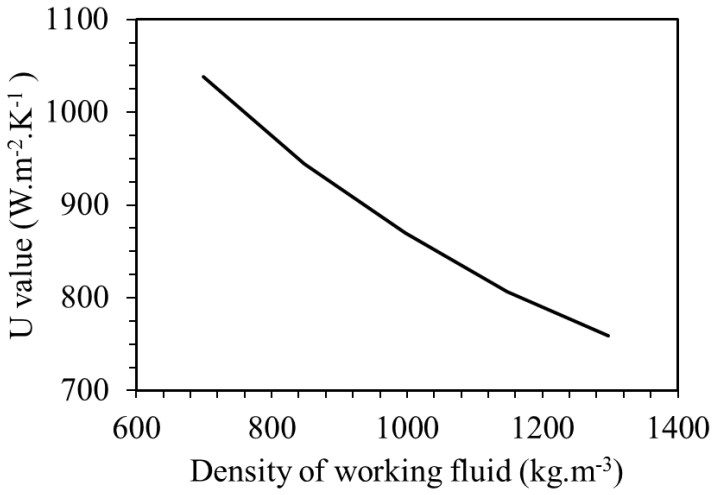

Figure 22. Sensitivity analysis on the density of the working fluid

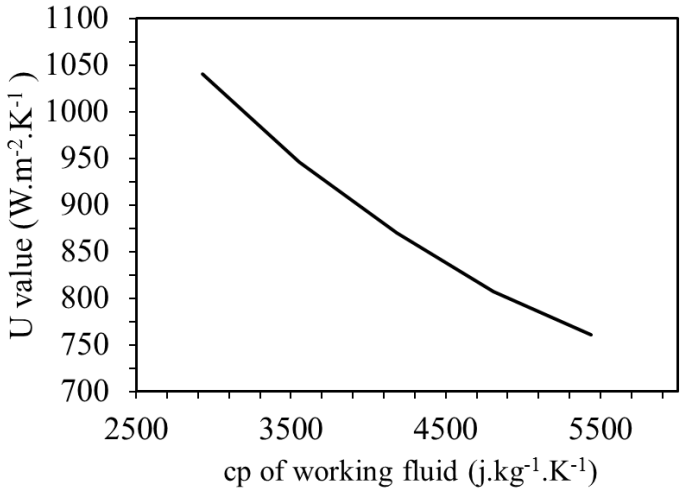

Figure 23. Sensitivity analysis on the c_p of the working fluid

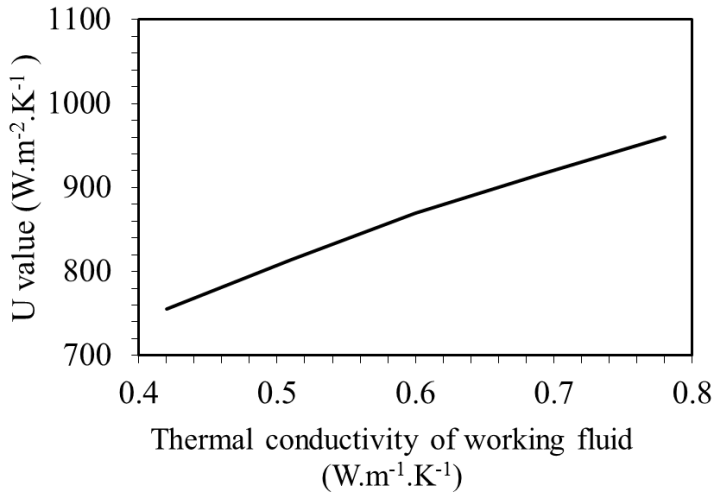

Figure 24. Sensitivity analysis on the thermal conductivity of the working fluid

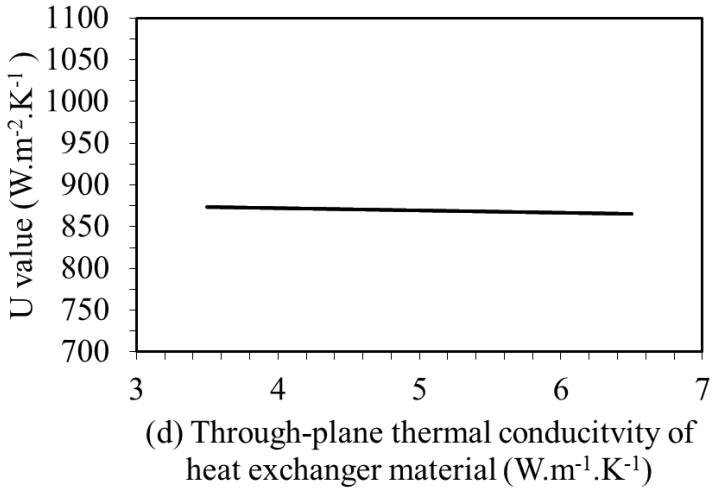

Figure 25. Sensitivity analysis on the through-plane thermal conductivity of the heat exchanger material

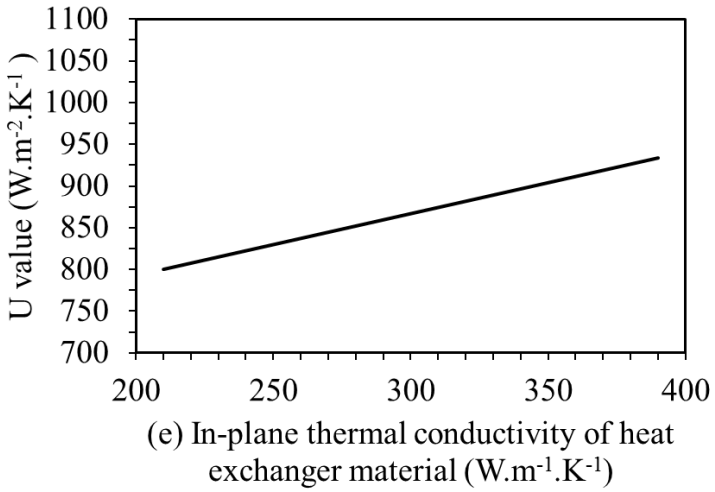

Figure 26. Sensitivity analysis on the in-plane thermal conductivity of the heat exchanger material

Results showed that properties of the fluid, such as specific heat, density, and thermal conductivity have a major effect on the U-value. Thus, increasing the thermal conductivity of the fluid would be the most effective way of enhancing the thermal performance of a heat exchanger. The properties of the heat exchanger material, such as in-plane and through-plane thermal conductivity, have less effect on the thermal performance. Interestingly the low through-plane thermal conductivity of graphite has a positive effect on the U-value. This showed that in such design, the anisotropic thermal conductivity of graphite has a slight advantage in thermal performance of the heat exchanger. It was seen that other input parameters such as viscosity of water, and density and specific heat of heat exchanger material do not have an effect on the U-value.

To further evaluate the thermal performance of G-HEX, a numerical model was used to compare graphite with the same aluminum heat exchanger. To do so, the heat exchanger's block material was set from graphite to aluminum while keeping the same geometry, boundary conditions, and fluid properties. Considering the input parameters of Table 9, the U-value of graphite and aluminum heat exchanger is compared in Figure 27. The numerical results suggest that G-HEX has 8.5% higher U-value compared to the same aluminum one.

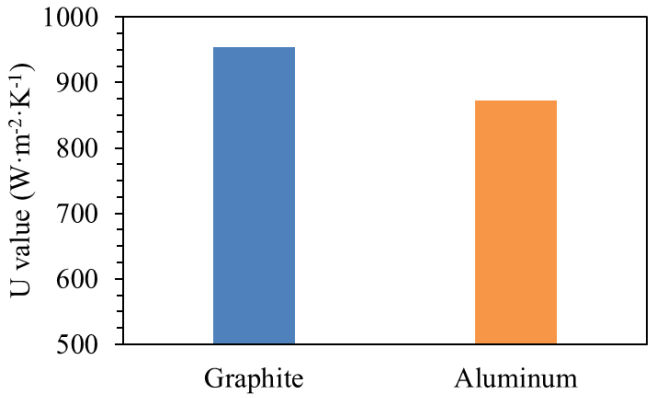

Figure 27. U-value comparison of graphite versus aluminum heat exchanger.

3.5 Off-the-shelf chevron-type plate heat exchanger

An off-the-shelf chevron-type plate heat exchanger was tested with the experimental setup for two purposes. First it is to compare the performance of graphite heat exchangers with the ones available in market, and second to validate the Nusselt number and friction factor correlations based on the literature review in the introduction section. These correlations will be used in the next chapter to perform an optimization study on chevron-type plate heat exchangers.

3.5.1 Experimental results

An off-the-shelf chevron-type brazed plate heat exchanger was chosen for this experiment. The geometrical design parameters of the heat exchanger are provided in Table 10.

Table 10. Design parameters of the tested chevron plate heat exchanger.

Parameter	Values
Plate length (Lp)	172 mm
Plate width (Lw)	76 mm
Enlargement factor (∅)	1.17
Number of plates (N)	10
Channel spacing	1.9 mm
Chevron angle (β)	30º

In this experiment, the flow rate was converted to Reynolds number using Eq. (8). Then by changing the flow rate and accordingly the Reynolds number, the Nusselt number was calculated for a range of Reynolds numbers, as shown in Figure 28. The graph also compared the experimental data with a few available correlations in the literature [15, 18, 19]. The experimental results showed a good agreement with the Chisholom et al. correlation which is shown in Eq. (9). The correlation also includes all the design parameters of the plate heat exchanger. Therefore, it is used for the Nusselt number calculation in the optimization code.

$$Nu = 0.72Re^{0.59}Pr^{0.4}\emptyset^{0.41}(\beta/30)^{0.66} \quad (9)$$

Where:

Pr= Prandtl number

∅ = Enlargement factor

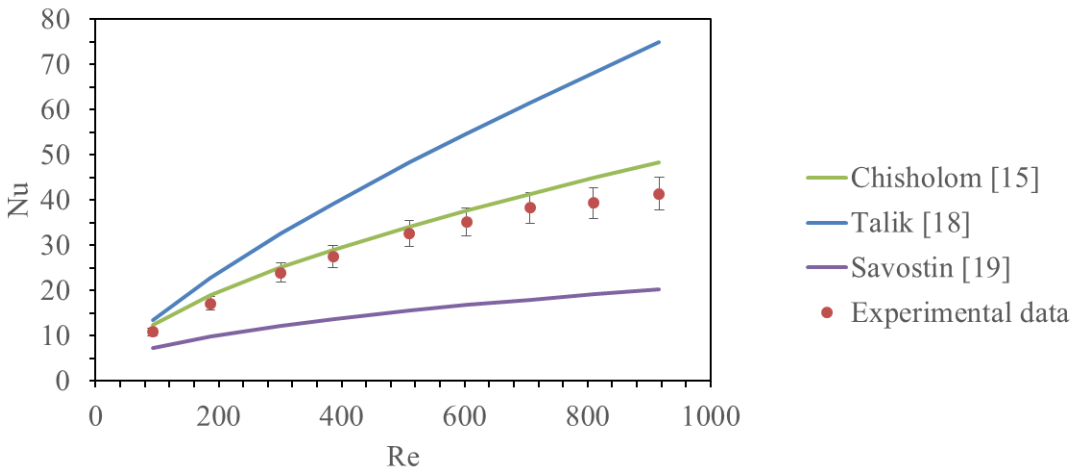

Figure 28. Comparison of Nusselt number at various Reynolds numbers.

As discussed, the pressure drop of a plate heat exchanger can be calculated from Eq. (9). In Fig. 25, the pressure drop was measured at various Reynolds numbers and compared to the calculated pressure drop. Each correlation in Figure 29 suggests a formula for calculating fanning friction factor [15, 18, 19]. The Savostin et al. correlation, showed in Eq. (10), considers all the design parameters and showed a good agreement with the experimental data [19]. This correlation is used for friction factor calculation in the optimization code.

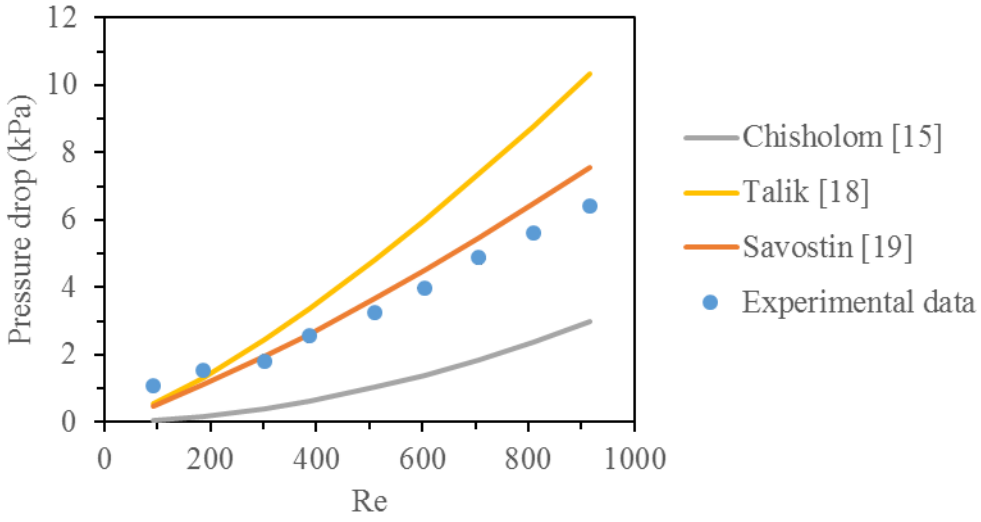

Figure 29. Comparison of pressure drop at various Reynolds numbers.

$$\mathrm{f} = 6.25(1 + 0.95(2\theta)^{1.72})\emptyset^{1.84}Re^{-0.84} \quad (10)$$

3.6 Graphite plate heat exchanger

As discussed in Chapter 2, one of the main motivations of graphite plate heat exchanger fabrication was to increase the heat transfer surface area compared to the layered G-HEX. In this section, the thermal and hydraulic performances of three types of heat exchangers are being compared with the experimental setup. It is concluded that the graphite plate heat exchanger offers a higher heat transfer rate compared to the layered G-HEX, however, its pressure drop is higher as compared to the off-the-shelf plate heat exchanger.

3.6.1 Experimental results

An experiment was conducted with identical inlet conditions on the three types of heat exchangers. The goal is to compare the U-value, total heat transfer rate, and pressure drop of

these three while having the same inlet conditions. The results of the experiment are shown in Figures 30, 31 and 32. The inlet conditions of the experiment are shown in Table 11.

Table 11. Inlet conditions for heat exchanger comparison test.

Experiment inputs	Value
Flow rate of hot and cold loop	1.4 lit.min^{-1}
Hot loop inlet temperature	45°C
Cold loop inlet temperature	15°C

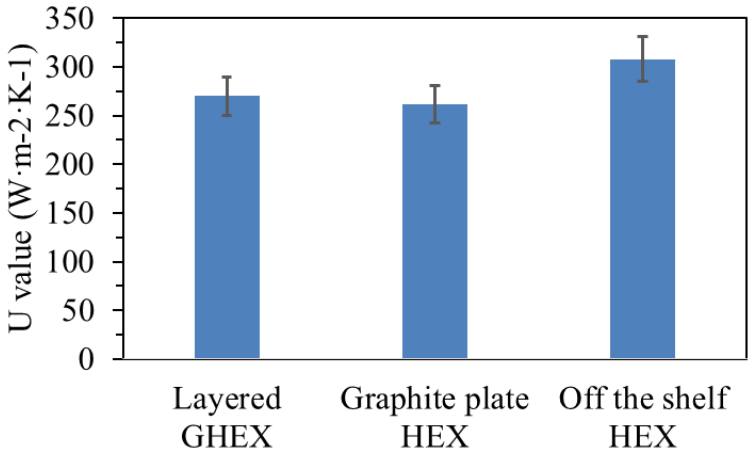

Figure 30. U-value comparison between layered G-HEX, graphite plate heat exchanger, and off-the-shelf heat exchanger.

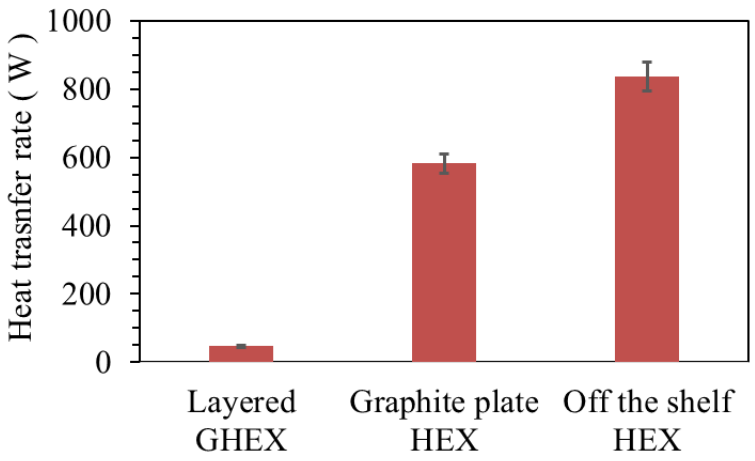

Figure 31. Heat transfer rate comparison between layered G-HEX, graphite plate heat exchanger and off-the-shelf heat exchanger.

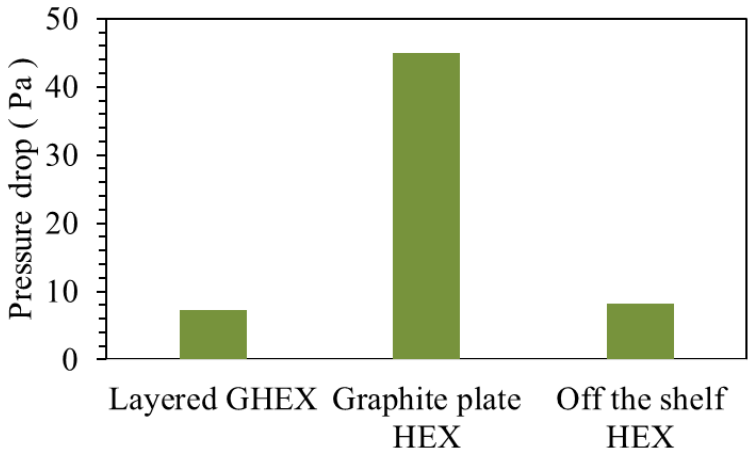

Figure 32. Pressure drop comparison between layered G-HEX, graphite plate heat exchanger and off-the-shelf heat exchanger.

According to Figure 30, the U-value of the graphite plate heat exchanger is lower than the other two. Although the difference in the thermal conductivity of the graphite in through-plane direction and in-plane direction is high, (300 $W.m^{-1}.K^{-1}$ versus 5 $W.m^{-1}.K^{-1}$), this had a minor decreasing effect on the U-value of the graphite plate heat changer. It can be concluded that in case of a water-water heat exchanger, in the thermal resistance network between the hot and cold fluid, which includes convective resistance of the hot fluid, conduction resistance of the plate, and convection resistance of the cold fluid, the conduction resistance of the plate is not the main resistance. Thus the lower thermal conductivity of the plate does not have a major effect on the

U-value. It can be seen that the off-the-shelf plate heat exchanger has higher U-value compared to the other two. This is due to the fact that its surface features and corrugations decrease the convection resistance of the hot and cold fluids.

As shown in Figure 31, the graphite plate heat exchanger showed a much higher heat transfer rate compared to the layered G-HEX. This was due to the significant increase in the heat transfer surface area. However, the heat transfer rate of the off-the-shelf heat exchanger is still higher than the graphite plate heat exchanger. As expected, the surface features of the off-the-shelf heat exchanger plates have increased the surface area as well as the U-value, resulting in a higher heat transfer rate.

From Figure 32, it can be seen that the pressure drop of the graphite plate heat exchanger is much higher than the other two. As it was mentioned in the literature review section, A. Durmus et al. showed that plate heat exchangers with corrugated plates have higher heat transfer rate and pressure drop compared to flat plates [11]. So it was expected that the off-the-shelf heat exchanger, due to its corrugated surface patters, has a higher pressure drop. But in the fabrication of the graphite plate heat exchanger, the rubber gaskets between the plates have squeezed by the pressure of tightening the bolts. This pressure resulted in the compression of the rubber gaskets so that the channels for the hot and cold fluids became narrower than the off-the-shelf plate heat exchanger. According to Eq. (9), a smaller channel area results in a higher pressure drop.

From the above observations, it can be concluded that there is still room to improve the thermal and hydraulic performance of the graphite plate heat exchanger by using thicker rubber gaskets and applying surface features on the graphite plates. The next chapter of this thesis is focused on finding an optimum design, to have a higher performance compared to the off-the-shelf plate heat exchanger in future designs.

Chapter 4. Optimization study on a plate heat exchanger

With the experiment results on the graphite plate heat exchanger, the goal of this chapter is to improve the thermal and hydraulic performance of the next design by adding surface patterns on the plates and choosing the optimum values for each design parameter. Chevron patterns are chosen for this purpose due to their performance superiority that is explained in the introduction chapter. The off-the-shelf plate heat exchanger is considered as a base for this optimization study. The accurate correlations for the Nusselt number and friction factor of a chevron-type plate heat exchanger has been found and validated with the water-water experimental setup as explained in Chapter 3. These correlations will be used for Nusselt number and friction factor calculation in the optimization section.

4.1 Optimization details

As discussed in the literature review section, enhancement of the plate surface area by adding surface patterns leads to a higher heat transfer rate but increases the pressure drop as well [11]. In order to consider both heat transfer and pressure drop at the same time, a parameter should be defined to have heat transfer and pressure drop with comparable units. In a compact heat exchanger design, surface goodness factor is a dimensionless parameter that is commonly used to consider heat transfer benefit over pressure drop cost as shown in Eq. (11) [27]. In the form of the total heat transfer energy gain over pressure drop, a coefficient of performance can also be defined as shown in Eq. (12).

$$Surface\ goodness\ factor = \frac{j}{f} = \frac{NuPr^{1/3}}{fRe} \tag{11}$$

$$COP = \frac{Heat\ transfer\ benefit}{pressure\ drop\ cost} = \frac{\dot{m}c_p\Delta T}{\dot{V}_h\Delta P_h + \dot{V}_c\Delta P_c} \tag{12}$$

Where:

$\dot{V}_h$= Volumetric mass flow rate of water in hot side ($m^3.s^{-1}$)

$\dot{V}_c$= Volumetric mass flow rate of water in cold side ($m^3.s^{-1}$)

The Nusselt number and friction factor in a plate heat exchanger are a function of the design parameter. Previously in Chapter 3, accurate correlations for Nusselt number and friction factor calculation were obtained and validated with the experimental setup. The correlations were shown in Eq. (9) for Nusselt number and Eq. (10) for friction factor. A code was written in MATLAB to calculate the Nusselt number and friction factor as a function of the design parameters.

According to Figure 7, the design parameters of a chevron-type plate heat exchanger are: plate width (Lw), plate length (Lp), corrugation depth (b) and chevron angle (β). In this study, an optimum heat exchanger is defined as the one having the highest surface goodness factor. To find the value of each design parameter that gives the highest surface goodness factor, MATLAB's genetic algorithm optimization tool was utilized. The default values for genetic algorithm options, including population size (= 50), crossover fraction (=0.8) and mutation option were used. It was seen that changing the default option values leads to the same result. As per different starting points, the solution converged in less than 5 seconds.

The heat exchanger is assumed to operate with water on both hot and cold sides. Table 12 shows the fluid inlet conditions used in the optimization code. The other fluid properties such as density, thermal conductivity, and viscosity are similar to the values in Table 9 [27].

Table 12. Fluid properties used for optimization.

Parameter	Values
Hot fluid	Water at 40ºC
Cold Fluid	Water at 20ºC
Mass flow rate	0.08 kg/s for both sides

A range was defined for each design parameter and the optimization code sought to find the optimum value for each parameter within the range. As the heat exchanger requires four ports to install the fittings, the plate width (L_w) should not be less than 65mm. The corrugation depth (b)

that defines the channel spacing also considered to be less than 2.5mm to avoid the bulkiness of the heat exchanger. The only constraint was that the total heat transfer surface area (plate length times plate width), or in other words the material use, considered to be the same as the off-the-shelf plate heat exchanger. The results of the optimization study, as well as upper and lower bounds are shown in Table 13.

Table 13. Optimum values of the design parameters within upper and lower bonds.

Design parameter	Upper bond	Lower bond	Off-the-shelf plate heat exchanger	Optimum design parameters
Lp (Plate length)	100 mm	300 mm	172 mm	198 mm
Lw (Plate width)	100 mm	65 mm	75 mm	65 mm
b (Corrugation depth)	1 mm	2.5 mm	1.9 mm	2.5 mm
θ (Chevron angle)	30°	80º	30º	30°

A comparison between the optimized heat exchanger and the test one shows that there is a 6.5% higher surface goodness factor in the optimized plate heat exchanger while using the same amount of material. This design also increases the coefficient of performance by a factor of 1.5. A schematic of the comparison is shown in Figure 33.

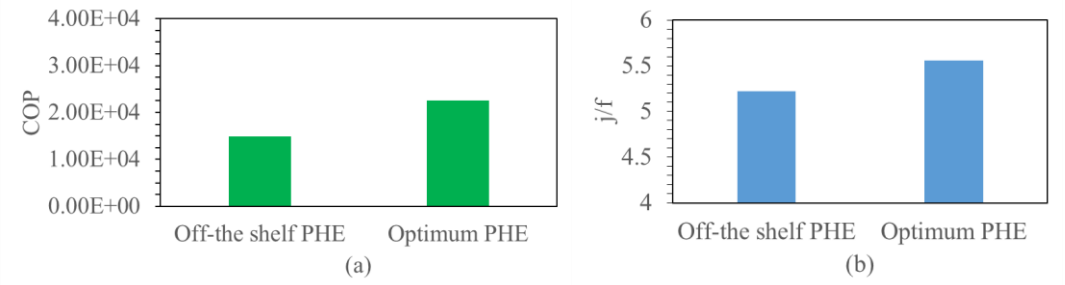

Figure 33. Comparison between optimum and off-the-shelf plate heat exchanger in terms of: (a) Coefficient of performance (COP); and (b) Surface goodness factor.

Chapter 5. Corrosion study on graphite

As mentioned in the introduction, one of the main advantages of graphite heat exchangers over metallic ones is their resistance to corrosion. To understand the potentials of utilization of graphite heat exchangers in corrosive environments, this chapter focused on the corrosion resistivity of natural graphite sheets. An experiment with sulfuric acid conducted on both resin impregnated and non-impregnated graphite sheets with two different densities to measure the corrosion rate of graphite. To check for any changes in surface structures after the acid test, Nano-SEM images were taken before and after the test.

5.1 Experiment details

Four types of samples were tested in this study: two non-impregnated samples, one with high and one with low density, and similarly two impregnated samples with high and low densities. For the validity of the test, three samples from each type were made. The samples were all made from the same starting graphite sheet with the density of 70 $g.cm^{-2}$ that was compressed down to 2mm and 1mm for the low and high density samples, respectively. The specification of the samples, including weights and densities are given in Table 14 for non-impregnated, and Table 15 for the impregnated ones.

Samples with diameter of 20 mm were placed in separate test tubes that were partially filled with sulfuric acid. The tubes were made from borosilicate glass which was resistant to corrosion (ASTM 438E). The duration of the test was one week (168 hours) with sulfuric acid at room temperature (25ºC).

Table 14. Non-impregnated graphite samples specifications.

Sample number	Thickness (mm)	Weight (g)	Density (g.cm^{-3})
1	2.0	0.2242	0.3568
2	2.0	0.2192	0.3489
3	2.0	0.2208	0.3514
4	1.0	0.2643	0.8413
5	1.0	0.2699	0.8591
6	1.0	0.2608	0.8302

Table 15. Resin impregnated graphite samples specifications.

Sample number	Thickness (mm)	Weight (g)	Density (g.cm^{-3})
7	2.0	0.7007	1.1152
8	2.0	0.7757	1.2346
9	2.0	0.6994	1.1131
10	1.0	0.4389	1.3971
11	1.0	0.4327	1.3773
12	1.0	0.4402	1.4012

In the following test, sulfuric acid was used at ambient temperature with concentration of 98%. According to American Society for Testing and Materials standard (ASTM), the corrosion rate was calculated using Eq. (12) [28].

$$Corrosion\ rate\ \left(\frac{mm}{year}\right) = \frac{Weight\ loss\ (g) \times 8.6 \times 10^4}{Material\ density\ (g.cm^{-3}) \times Exposed\ area\ (cm^2) \times Exposure\ time\ (hr)} \quad (12)$$

5.2 Experiment results

After the one-week test, it was seen that the impregnated samples had chemical reaction with sulfuric acid. As a result, graphite flakes were fallen apart and spread in the solvent as it can be seen in Figure 34. On the other hand, non-impregnated samples kept the original shape. The weight measurements after the test showed a significant increase in the samples weight which was due to adsorption of acid. To evaporate the adsorbed acid, samples were kept in oven for 3 hours under 200ºC.

Table 16 shows the wet and dry weight measurements after the test. According to the table, there was no weight reduction in non-impregnated samples as a result of corrosion within the accuracy of 10^{-4} grams. Some of the samples however, had a very small increase in weight. This is due to the fact that during the rinsing process, although samples were carefully rinsed and dried, small amounts of sulfuric acid salts remained in some of them. This weight increase was in order of 10^{-4} grams. To make a comparison, if samples with the same dimensions were made from austenitic stainless steel, with the same testing condition they had a corrosion rate of 0.11 mm per year which leads to a 0.013 gram weight reduction after one week [31]. This proves the fact that non-impregnated graphite is resistant to corrosion when exposed to 98% concentration sulfuric acid at ambient temperature.

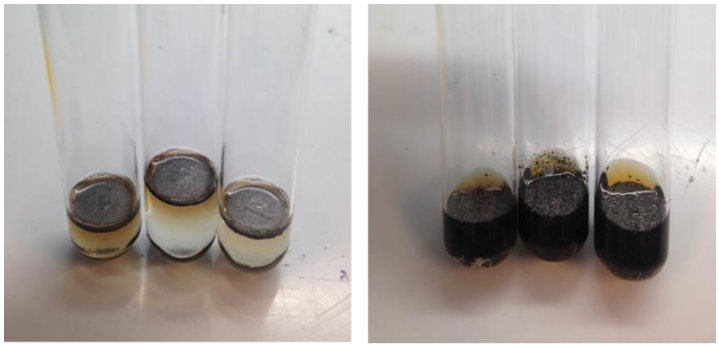

Figure 34. Samples after one-week test in sulfuric acid: a) Non-impregnated graphite; and b) Impregnated graphite.

Table 16. Wet and dry weight of non-impregnated graphite samples after acid test.

Sample number	Initial weight (g)	Wet weight after acid test (g)	Dry weight after acid test (g)
1	0.2242	1.3670	0.2245
2	0.2192	1.4110	0.2204
3	0.2208	1.4535	0.2227
4	0.2643	0.7614	0.2645
5	0.2699	0.7713	0.2705
6	0.2608	0.7580	0.2609

To observe the potential changes in the surface of the samples, Nano-SEM images were taken before and after the test. The images were taken with Nova NanoSEM 430 in three magnifications of 300X, 3000X and 30000X as shown in Figure 35 for low density samples and Figure 36 for high density ones. The comparison showed that there are more bright colors in samples after the acid test, which was due to the presence of sharper edges. This confirms that the roughness of the samples was increased after the acid test which can be caused by exfoliation of graphite in sulfuric acid [29]. However, since the net weight of the samples was not changed during the test, this phenomenon cannot be due to pit corrosion.

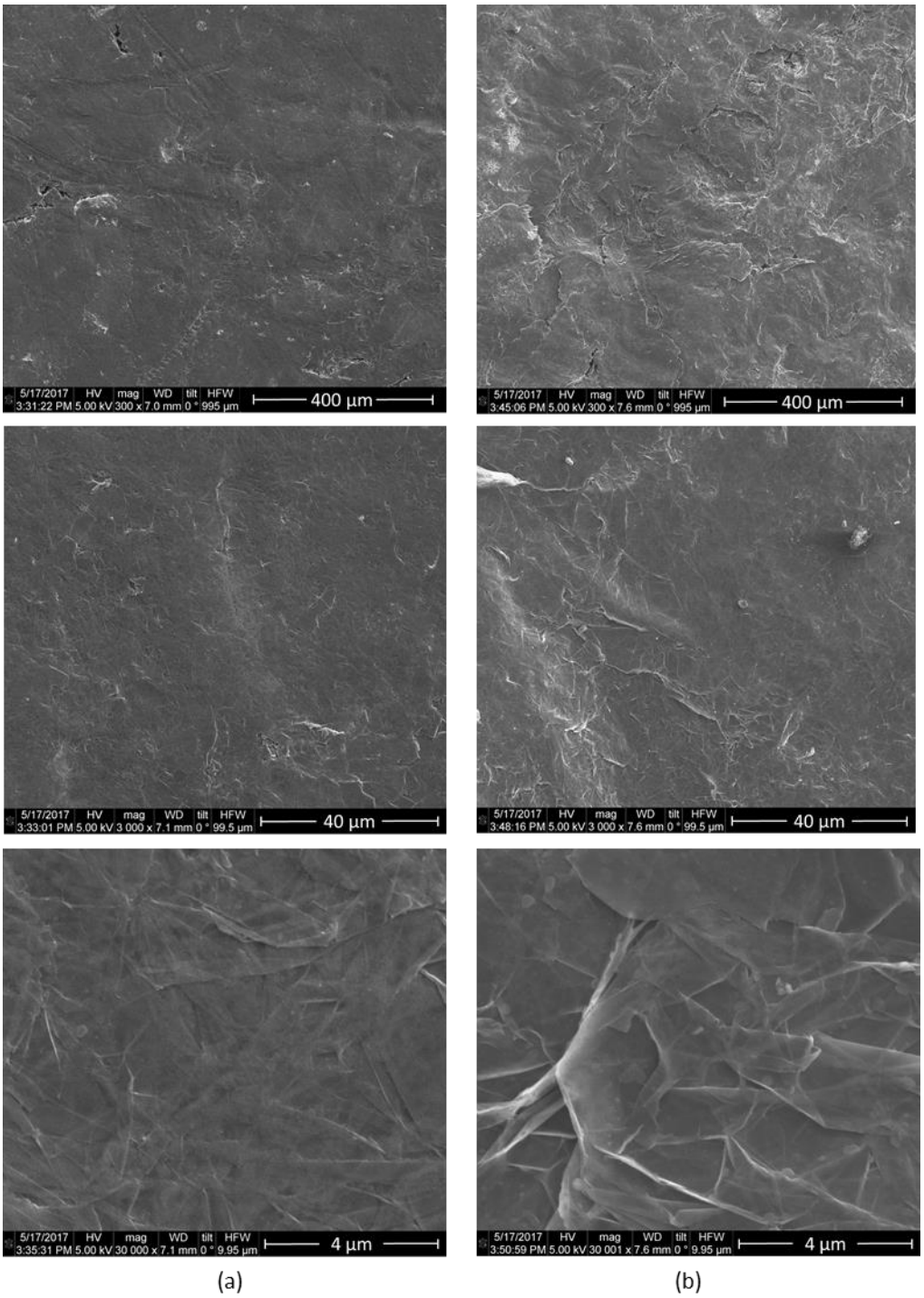

Figure 35. Nano-SEM images of the surface of 0.35 gr.cm-3 graphite a) Before acid test; and b) After acid test.

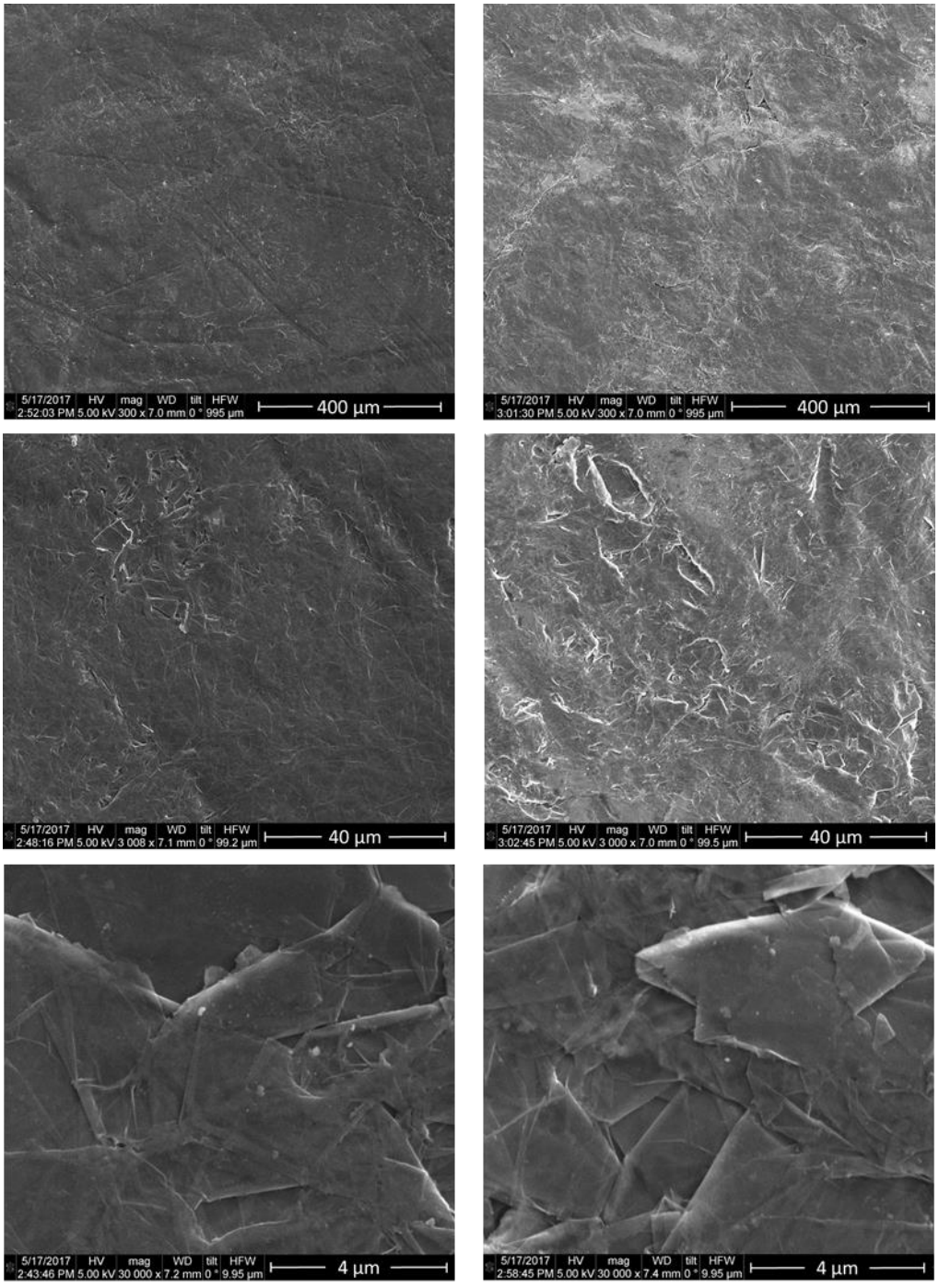

Figure 36. Nano-SEM images of the surface of 0.84 gr.cm-3 graphite a) Before acid test; and b) After acid test.

Chapter 6. Conclusions and future work

Novel methods for fabrication of graphite-based heat exchangers from natural graphite sheets were suggested. A layered G-HEX and a graphite plate heat exchanger were designed and fabricated. Their thermal and hydraulic performance were compared to an off-the-shelf plate heat exchanger using a water-water experimental setup. A numerical model of the layered graphite heat exchanger was then developed and validated with the experimental results. The model confirmed that the thermal performance of a heat exchanger is highly sensitive to the properties of the working fluid such as thermal conductivity, density and specific heat and is less sensitive to the thermal conductivity of the heat exchanger material. The model also proved an 8.5% improvement in U-value of the graphite heat exchanger compared to an aluminum one.

To prove the corrosion resistivity of natural flake graphite, a corrosion test with 98% concentration of sulfuric acid at ambient temperature was conducted for the duration of 168 hours. The weight measurements with accuracy of 10^{-4} grams before and after the test showed that the corrosion rate of graphite in sulfuric acid is equal to zero. However, the graphite samples that were impregnated with Hernon® Porosity Sealant (HPS) 991, dissolved in the sulfuric acid. As resin impregnation process can increase the mechanical strength of graphite sheets and operating pressure of graphite heat exchangers. Finding a corrosion resistant resin would be a next step for this study.

As noted, the acid test was conducted at ambient temperature. But in some heat exchanger applications the corrosive fluid is at a higher temperature. Therefore, investigating the corrosion resistivity of graphite at elevated temperatures would be another next step. An experimental setup for this test was chosen and is shown in figure 38 of the appendix.

The optimization study on chevron-type plate heat exchanger suggested a set of design parameters to improve the surface goodness factor of the next generation of graphite plate heat exchangers. The optimization results showed a potential of 6.5% improvement in surface goodness factor and 150% improvement in COP of the future design. A set of dies for the fabrication of the chevron-type graphite plate heat exchangers were designed as shown in Figure 37. The drawings of this design are brought in the appendix (Figures 39 and 40). Fabrication and test of this heat exchanger is another future work of this study.

Figure 37. Dies for fabrication of optimized chevron-type graphite plate heat exchanger.

References

[1] http://www.marketsandmarkets.com/PressReleases/heat-exchanger.asp , August 2017.

[2] M.P. Schwartz, “Four types of heat exchanger failures”, Plant Engineering, Dec 23:45-50, 1982.

[3] R.G. Ripeanu, "Design and technology parameters influence on durability for heat exchangers tube to tubesheet joints." *IOP Conference Series: Materials Science and Engineering*. Vol. 174. No. 1. IOP Publishing, 2017.

[4] S. Kakac, H. Liu, A. Pramuanjaroenkij, “Heat exchangers: selection, rating, and thermal design”, CRC press, 2012.

[5] E.G. Acheson, "Manufacture of graphite.", U.S. Patent No. 568,323, 1896.

[6] Alfa Laval DIABON® graphite plate heat exchanger PPI00556EN1304 product technical data sheet, Alfa Laval, Lund, Sweden, 2014.

[7] M. Wankhede, V. Khaire, A. Goswami, “Evaluation of cooling solutions for outdoor electronics”, 13th Int. Conf. Thermal Investigation of ICs and Systems, p. 1, 2007.

[8] S. Kohlenstofftechnik, “Manufacturing Process and Material Properties of Carbon and Graphite Materials’, www. schunk-group.com, 2004.

[9] E. Pop, V. Varshney, A.K. Roy, “Thermal properties of graphene: Fundamentals and applications”, MRS bulletin. 37(12):1273-81, 2012.

[10] R. K. Shah, W. W. Focke, "Plate heat exchangers and their design theory", Heat Transfer Equipment Design 227: 254, 1988.

[11] A. Durmuş, H. Benli, İ. Kurtbaş, H. Gül, “Investigation of heat transfer and pressure drop in plate heat exchangers having different surface profiles”, International journal of heat and mass transfer, 28;52(5):1451-7, 2009.

[12] D. Dović, S. Švaić, “Influence of chevron plates geometry on performances of plate heat exchangers”, Tehnicki vjesnik/Technical Gazette 14, 2007.

[13] J. Yin, G. Yang, Y. Li, “The effect of wavy plate phase shift on flow and heat transfer characteristics in corrugated channel”, Energy Procedia 14: 1566-1573, 2012.

[14] G. A. Longo, A. Gasparella, R. Sartori. "Experimental heat transfer coefficients during refrigerant vaporisation and condensation inside herringbone-type plate heat exchangers with enhanced surfaces", International Journal of Heat and Mass Transfer 47.19: 4125-4136, 2004.

[15] D. Chisolm, A. S. Wanniarachchi, "Maldistribution in single-pass mixed-channel plate heat exchangers" *ASME, New York,* 201: 95-99, 1992.

[16] H. Martin, “A theoretical approach to predict the performance of chevron-type plate heat exchangers”, Chem. Eng.Process. 35: 301–310, 1996.

[17] A. Maslov, L. Kovalenko, “Hydraulic Resistance and Heat Transfer in Plate Heat Exchangers", Molochnaya Promyshlenflost, 10: 20-22, 1972.

[18] A.C. Talik, “Heat Transfer and Pressure Drop Characteristics of a Plate Heat Exchanger”, ASME, NewYork, 1995.

[19] A.F. Savostin, A. M. Tikhonov. "Investigation of characteristics of plate-type heating surfaces" Thermal Engineering 17.9: 113, 1970.

[20] V. Dvořák, "A method for optimization of plate heat exchanger" , 18th International Conference on Circuits, Systems, Communications and Computers, Santorini Island, Greece, 2014.

[21] K. Guo, “Optimisation of plate/plate-fin heat exchanger design”, School of Chemical Engineering and Analytical Science, University of Manchester, 2015.

[22] H. Khond, D. Saurabh, K.V. Mali, “Design optimization algorithm for plate heat exchanger", International journal of current engineering and technology, E-ISSN 2277 – 4106, 2016.

[23] O.P. Arsenyeva, L.L. Tovazhnyansky, P.O. Kapustenko, G.L. Khavin, "Optimal design of plate-and-frame heat exchangers for efficient heat recovery in process industries", *Energy* 36.8 :4588-4598, 2011.

[24] M. Kan, O. Ipek, B. Gurel. "Plate heat exchangers as a compact design and optimization of different channel angles", Special issue of the International Conference on Computational and Experimental Science and Engineering, *Acta Physica Polonica A* 12: 49-52, 2015.

[25] J.M. Pinto, J. A. W. Gut. "A screening method for the optimal selection of plate heat exchanger configurations." *Brazilian Journal of Chemical Engineering* 19.4: 433-439, 2002.

[26] J. P. Holman, “Experimental Methods for Engineers”, McGrawHill, New York, 2001.

[27] F. P. Incropera, D.P. DeWitt, T.L. Bergman, “*Fundamentals of heat and mass transfer”,* J. Wiley & sons, 2007.

[28] ASTM G1-81, "Preparing, Cleaning, and Evaluating Corrosion Test Specimens," American Society for Testing and Materials, Philadelphia, PA.

[29] M. Inagaki, R. Tashiro, Y.I. Washino, M. Toyoda, “Exfoliation process of graphite via intercalation compounds with sulfuric acid”, Journal of physics and chemistry of solids, 31;65(2):133-7, 2004.

[30] P. Jamzad, M. Ahmadi, M. Bahrami, “Performance Evaluation of a New Layered Graphite Heat Exchanger”, ASME Summer Heat Transfer Conference, 2017.

[31] L. Iliyasu I, D. S. Yawas, S.Y. Aku, “Corrosion Behavior of Austenitic Stainless Steel in Sulphuric Acid at Various Concentrations”, Department of Mechanical Engineering, Ahmadu Bello University Zaria, Nigeria, 3(6):3909-3915, 2012.

Appendix

The testbed for the elevated acid test is shown in Figure 38. It consists of a dry electric block heater, a sand bath and a set of test tubes. The graphite samples are put in the test tubes that are filled with acid, and the tubes are placed in the sand bath. The sand bath is mounted on the block heater. By manually increasing the heating power of the heater, elevated temperatures of acid can be reached.

Figure 38. Acid testbed for elevated temperatures, a) Sand bath, b) Dry block heater

The drawings for the first version of the chevron-type graphite plate heat exchanger are shown in Figure 39 and 40.

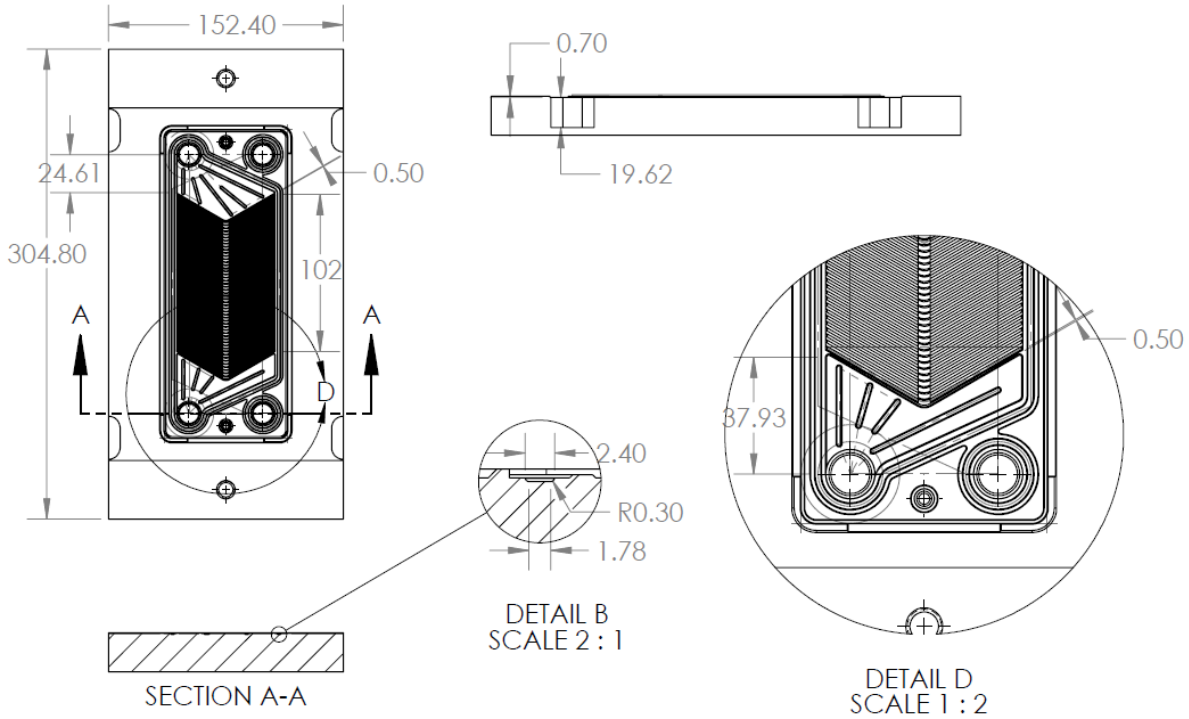

Figure 39. Drawing of the chevron-die for graphite plate heat exchanger (a)

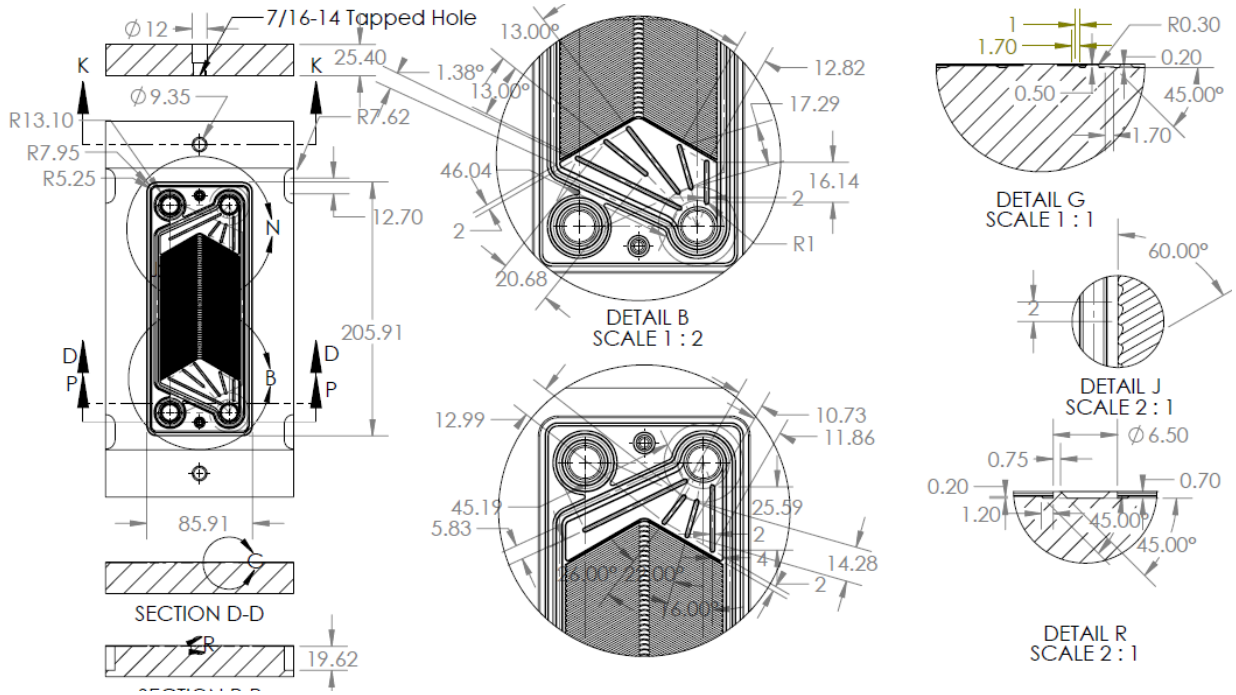

Figure 40. Drawing of the chevron-die for graphite plate heat exchanger (b)